Rheological implications of extensional detachments: Mediterranean and numerical insights

Loic Labrousse, Benjamin Huet, Laetitia Le Pourhiet, Laurent Jolivet, Evgenii E.B. Burov

Rheological implications of extensional detachments : Mediterranean and numerical insights.

Loïc Labrousse (1,2), Benjamin Huet (3), Laetitia Le Pourhiet (1,2), Laurent Jolivet (4) and Evgenii Burov (1,2).

1- Sorbonne Universités, UPMC Univ Paris 06, UMR 7193, Institut des Sciences de la Terre Paris (iSTeP), F-75005 Paris, France

2- CNRS, UMR 7193, Institut des Sciences de la Terre Paris (iSTeP), F-75005 Paris, France

3- Department of Geodynamics and Sedimentology U.Vienna Althanstrasse 14/2A273 A-1090 VIENNA

4- ISTO, UMR 6113 - CNRS/U. Orléans, 1A, rue de la Férollerie F-45071 ORLEANS

Abstract

The Mediterranean realm shaped by extensive back-arc extension after multiple collisions between Europe and isolated continental blocks is the second densest occurrence of Metamorphic Core Complexes (MCC) after the North American Cordillera. The present review aims at determining the factors controlling detachment system development during post-orogenic extension in the continental lithosphere. 26 different detachment zones over 23 different localities are systematically described and show that MCC structures can be positioned in a three end-member classification. Beside the high-temperature lower plate end-member, most of the time considered as the archetypical MCC type, two cold end-members can be identified: a first one preserving high pressure metasedimentary units in the vicinity of the detachment and represented by numerous cases in the Mediterranean and a second theoretical one with strain localized at the bottom of a resistant upper crust. These two end-members show a strain

pattern guided by inheritance more than thermal state. The relevance of this three end-member classification is then tested via numerical modelling of extension of layered continental lithosphere. The compilation of our results and recently published similar models show that over a 100 of different simulations the most critical parameter for developing a MCC is the intra-crustal strength contrast (S_{max}/S_{min}, where S_{max} and S_{min} stand respectively for the maximum – at the brittle-ductile transition – and minimum – at the Moho – crustal strength). This contrast has to be risen only by 1 order of magnitude to change extension mode. Below a critical value of 1000, narrow and wide rifts develop. MCCs with a perennial detachment are produced for values slightly higher than 1000, while higher intra-crustal strength contrasts systematically promote double-domes MCCs, with strain progressively relocalizing within the lower plate. Inherited layering is as efficient as temperature for raising this intra-crustal strength contrast while strain rate is actually a second order parameter. Metamorphic reactions are also to be considered as a first order process in localizing detachments.

1. Introduction

Even if the seminal comprehensive descriptions of Metamorphic Core Complexes (MCCs) in the American Cordillera mentioned lower plates constituted of gneiss and intruded by granites (Snake Range, Miller et al. (1983), Whipple Mountains, Davis et al. (1986), the actual definition of MCCs: « *Cordilleran metamorphic core complexes appear to be bodies from the middle crust that have been dragged out from beneath fracturing and extending upper crustal rocks, and exposed beneath shallow-dipping (normal slip) faults of large areal extent* » (Lister and Davis, 1989) refers to rocks exhumed from the middle crust whatever their thermal history. The fundamental property of this middle crust resides in its ability to flow lateraly toward the forming dome (Block and Royden, 2010), to accommodate stretching of the upper plate and preserve a relatively flat Moho (Figure 1). Even though thermal reequilibration can induce weakening of the lower crust (Buck, 1991) and increases its ability to flow below a relatively strong upper crust, a similar strength profile can also be inherited from pre-extension evolution of the continental crust and promote development of the original structure leading to the formation of MCCs: the detachment (Davis, pers comm.). In order to unravel the rheological meaning of detachments, we propose here a review of extensional shear zones described as post-orogenic detachments in the Mediterranean realm. These examples share a common tectonic setting and often affect comparable lithotectonic successions. A three end-members typology is proposed with high-temperature MCCs (HT end-member) as one end-member, and two cold MCC end-members with a weak middle crust due in most cases to the interlayering of high-pressure metasedimentary nappes during syn-orogenic wedge building (HP end-member). Even if not met in natural cases, a second theoretical cold end-member can be defined by the presence of a strong upper crust also due to nappe stacking or even obduction (HS end-member). In both cases, the inherited tectonostratigraphy is responsible for a sensible exaggeration of the intra-crustal strength contrast.

Fully coupled thermo-mechanical modeling experiments allow testing these three end-member typologies and determining the critical intra-crustal strength constrast for the perennial development of a detachment zone and building of a dome at the expense of the lower plate. The comparison of natural cases classification and model-based categories demonstrates the mechanical feasibility of all natural combinations and possibly explains how long-lasting multiple detachment systems such as Menderes, Turkey or North Cycladic Detachment System, Cyclades, Greece, evolve.

2. Mediterranean Extensional Detachments

Metamorphic Core Complexes are described in the Mediterranean within three large extended domains (Carpathians and Pannonian basin, Western Mediterranean from Alboran to Tyrrhenian, and Aegean domain *sensu lato*) subject to slab retreat during Alpine orogeny (Jolivet et al., 2009a). Most of them are now located in continental domains with Moho depths between 25 and 20 km, but not systematically in flat Moho areas (Figure 2). Betic Cordilleras and Menderes are, for instance, on top of dipping Moho with about 10 km vertical drop across them (Karabulut et al., 2013 for instance for Menderes). Metamorphic rocks exhumed within Mediterranean core complexes show a wide scatter in pressure-temperature conditions (Figure 3 and Table 1). Dating peak metamorphic conditions and detachment mylonites or relative dating of the detachment activity allow deciphering between rocks mostly exhumed during pre-extensional thickening stages from rocks exhumed during extensional dynamics leading to the MCC formation. Furthermore, the presence in the footwall of detachments of lower grade rocks structurally below the High Temperature and Low Pressure (HT-LP) or High Pressure and Low Temperature (HP-LT) rocks is also a criterion to attribute the first stages of the exhumation of the latter to syn-orogenic nappe stacking rather than lithospheric extension. Nappe stacking is indeed the sole process prompt to thrust high-grade metamorphic units on top of a preserved lower grade unit. For instance, the equilibration of the Ichendirene HP-granulite bodies (BB1, Figure 3) included in the lower grade Beni Bousera kinzigites (BB2, Figure 3) in Morrocco relates to stages earlier than the exhumation of the massif itself (Michard et al., 2006).

Even when removing HP-LT peaks inherited from pre-extensional stages and preserved during dome formation, the scatter of PT conditions sampled by detachments footwalls remains high. Noteworthy, some core complexes such as the one described in the Catena Costiera, Calabria, Italy (CC on Figure3, Rossetti et al. (2004), or in the Northern Cyclades (Tn, Tinos, Jolivet et al. (2010b) and references therein) show « cold » footwalls, with conditions theoretically uncompatible with the development of detachment systems, according to numerical models (Tirel et al., 2008). The rheological meaning of such « cold MCCs » (Huet et al., 2010), is the purpose of our study.

2.1 Tectonostratigraphic positions

The systematic description of tectonostratigraphic positions of Mediterranean detachments allows highlighting the preferred decoupling levels within the continental crust during its extension (Table 1 and 2). Among relevant characteristics, some were considered necessary for defining a detachment zone in our compilation: the presence of mylonites along the extensional fault system, in order to compare structures initiated below the ductile-brittle transition only, and a clear extensional setting, in order to compare post-orogenic extensional detachments only, and avoid exhumation shear zone (syn-orogenic detachments in Jolivet et al., 2003). Some characteristics differ from a detachment system to another: the lithology and PT conditions recorded by their footwall (patterns and color code on Figure 4), the lithology of their hangingwall, as well as the presence of plutons, with mantle or crustal origin. The presence of migmatites in the footwall has also been systematically noted. The initiation context of the exhumation process has also been checked : syn-orogenic for rocks partly exhumed during convergence, post-orogenic for rocks exhumed only during post-orogenic extension. The systematic documentation of those characteristics (Figure 4 and Table 2) shows a distribution of natural cases with three theoretical end-members, between which they can be positioned in a triangular diagram (Figure 5). The position of each case was deduced from the relative weighing of high temperature criterion (migmatites or high temperature lower plate or syn-kinematic intrusives), low temperature criterion (preservation of HP-LT paragenesis in the footwall) or high strength upper plate criterion listed in table 2. As will be discussed further, meditteranean natural cases plot within and along edges of the proposed ternary plot. While the HT and HP end-embers are represented by numerous natural cases, no case is found on the HS end-member. None of the documented examples indeed has a strong upper plate as single criterion.

2.1.1 Detachments on top of High-Temperature lower plates

Some of the Mediterranean detachments cap high-temperature lower plates, with HT-LP metamorphic rocks showing syn-extensional pervasive amphibolite facies metamorphism, possibly associated to migmatization, and/or syn-kinematic granite intrusion.

The Kabylian Detachment, Greater Kabylia, Algeria (KaD, table 1C), is located between Permian phyllites in its hanging-wall and amphibolite facies micaschists and orthogneisses in its footwall (Saadallah and Caby, 1996). Migmatitic textures, syn-tectonic aplitic dikes and late peraluminous granite intrusions indicate a temperature above the computed solidus (i. e. 700°C) during the exhumation of paragneiss and micaschists forming most of the lower plate. Rheological contrast between upper and lower plate is mostly due to contrasted thermal histories. The Edough massif (Ed, table 1D) in Algeria shows a similar structure (Caby et al., 2001) on top of various high grade metamorphic rocks reaching anatexis and intruded by syn-kinematic leucogranites. Fragments of sublithospheric mantle were incorporated within crustal stack and now constitute rheologically constrated inclusions (Bosch et al., 2014). Even if exhumation ages in the Edough massif are younger than in Greater Kabylia (Bruguier et al., 2009), both extensional domes actually built from the same crustal stack during Alboran slab retreat or later slab related dynamics.

On Elba island, Italy, even though the cataclastic low angle normal Zuccale fault zone accommodated substantial extension (Collettini and Holdsworth, 2004), the proper detachment zone (Capanne Detachment Zone, Table1H), exhuming the lower Tuscan unit greenschists, is located at the top of the syntectonic Monte Capanne granodiorite (Daniel and Jolivet, 1995). Mylonites are described in its thermometamorphic aureole and localization of strain is related to its intrusion.

The Lubenik Line (LL, table 1L), in the Central Western Slovakian Carpathians and the Zaouia Fault Zone, in the Beni Bousera massif, Morocco, even though both considered as structures inherited from orogenic stages (Janák et al., 2001; Michard et al., 2006) also belong to the High Temperature detachments class. In the Lubenik Line footwall, the Veporic unit is intruded by the syn-kinematic Rochovce granite and mylonites localized strain at its top (Janák et al., 2001). In the Beni Bousera massif, amphibolite facies metamorphism in the Fillali schists and associated kinzigites indeed indicate temperatures higher than 800°C for their peak conditions, and leucogranite intrusions evidence partial melting of the lower plate (Michard et al., 2006).

HT lower plate detachment class is therefore represented by detachment zones that exhume HT metamorphic rocks, which reached peak P-T conditions just before exhumation or lower plate intruded by plutons, responsible for local thermal weakening and strain localization. This mechanism is discussed in section 4.2.3.

2.1.2 Detachments within interlayered high-pressure metamorphic nappe

Most of the "Cold MCC" (Huet et al., 2010) exhume HP-LT metamorphic rocks in their footwall (Figure 3). Even though most of these HP-LT rocks were actually partly exhumed prior to the proper detachment tectonics related to extension, their preservation from thermal reequilibration during ultimate decompression implies that no significant thermal reequilibration occurred during MCC formation. Detachments faults described in the Betics, Spain (Mecina-Filabres Shear Zone, MSFZ, table 1A), on Syros, Greece (Vari detachment, VaD, table 1P), in southern Italy (Catena Costiera and Aspromonte, CatCo and Asp, table 1E & F), in Peloponnese, Greece and Crete (Cretan detachments 1 and 2, CrD1 and CrD2, table 1U &V) and also in the Rechnitz window, Austrian Alps (ReW, table1K) belong to this category.

The Mecina-Filabres Shear Zone develops as mylonites and gouges during extensional reactivation of a former thrust (Platt et al., 1984). Eclogites are preserved within the Nevado-Filabrides lower plate, and most of the syn-tectonic metamorphism is actually greenschist facies (Augier et al., 2005b). No drastic lithological contrast is observed between the upper plate Alpujarrides phyllites, quartzites and graphitic micaschists and the exhumed Bedar-Macael graphitic schists.

The Vari detachment, Syros, exhumes the Cycladic blueschist metasedimentary unit dominated by schists and marble preserving eclogite to blueschist paragenesis, (Trotet et al., 2001), beneath the Vari and "Upper unit" metabasites gneiss and serpentinites which experienced earlier HT reequilibration (Jolivet and Brun, 2008). Even if mainly syn-orogenic, this detachment may have been active in the late stages of post-orogenic extension (Jolivet et al., 2010a).

In Italy, the Catena Costiera detachment is described as a mylonites and cataclasites complex, accounting for the post-orogenic exhumation of the blueschist-bearing metaclastics and marbles associated to the Lower Ophiolitic Unit (LOU, Jolivet and Brun, 2008; Rossetti et al., 2004) beneath the seemingly Upper

Ophiolite Unit, composed of an ophiolitic melange and carbonates (Bonardi et al., 2001). The Aspromonte detachment is a mylonite zone located on top of the Alpine blueschist Apromonte unit, considered as a syn-to immediate post-orogenic structure (Heymes et al., 2010). Aspromonte and Stilo units on both sides of the detachment are both composed of para and orthogneiss.

Cretan detachments, described on top of the blueschist facies Phyllites-Quartzites nappe in northern Peloponnese (Jolivet et al., 2009b) and in Crete (Kilias et al., 1994) are represented by extensional mylonites and high-strain phyllites along the reactivated thrust at the base of the Gavrovo-Tripolitza nappe in Crete, or the underlying Tyros Beds in Peloponnese.

In the Rechnitz window group, the detachment zone is composed of serpentinites and quartz-micas mylonites (Cao et al., 2013) at the base of the Austro-Alpine greenschist facies Wechsel unit, and at the top of the blueschist-bearing Rechnitz Penninic unit. A limited HT imprint is recorded during the inferred post-orogenic reactivation of the Austro-Alpine basal thrust (Hoinkes et al., 1999).

All the detachment detailed above are therefore located within a tectonostratigraphic sequence with no significant systematic strength contrast, upper and lower plate being most of the time similar in lithologies, except the HP paragenesis partly preserved in lower plates. Most of the time, extensional strain localized on a former thrust. The reason why such thrusts are prone to extensional reactivation will be discussed further.

2.1.3 Detachments at the base of a strong upper crustal unit

Two close classes of detachment emerge from this review: some localize at the base of a strong upper plate and on top of a HP preserving cover unit and some at the base of a strong upper plate on top of a HT lower plate.

In Nigde massif, Turkey (NiD, table 1W) the amphibolite facies Gumusler formation migmatites (Whitney and Dilek, 1997) are exhumed beneath a massive ophiolite mostly composed of greenschist-facies gabbros (Goncuoglu et al., 1991). Mylonites and cataclasites developed prior to the Uçkapili leucogranite intrusion (Gautier et al., 2002) during an early extension stage affecting the Central Anatolian continental block.

In southern and eastern Rhodope (Bulgaria-Greece), the Kerdylion detachment and the Tokachka and Kechros detachment system (KerD and ToKeD, table 1M & N) developed at the base of high-grade rock units: the Vertiskos Gneiss complex (Brun and Sokoutis, 2007) and the Kimi complex garnet-bearing gneiss (Bonev and Beccaletto, 2007) respectively. They exhume the Southern Rhodope Core Complex, the Kesebir-Kardamos and Kechros complexes, all of them being represented by migmatites (Bonev et al., 2006) and amphibolite facies orthogneiss intruded by syn-kinematic granitoids (Vrondou and Symvolon granodiorites in Southern Rhodope, and the Papikjon granitoid in Eastern Rhodope). The base of upper plates is underlined by resistant lithologies such as the Therma and Volvi gabbros and basalts in Southern Rhodope or meta-ophiolitic lenses in Eastern Rhodope (Burg et al., 1996).

The Motajica Detachment, Croatia-Bosnia Hercegovina (MoD, table 1, Ustaszewski et al. (2010) is located at the base of the Tisza-Dacia unit ophiolite and at the top of an amphibolite facies meta-accretionary wedge complex intruded by the Motajica granite a few Myr prior to extension initiation (Pamić et al., 2012).

In Kazdag, Turkey, extension localized along the northern Alakeçi and southern Selale detachments (AlSeD,table 1S). Mylonites, metaserpentinites and breccias separate the upper plate Cetmi ophiolitic melange from an amphibolte facies basement unit (Beccaletto and Steiner, 2005; Okay and Satir, 2000) topped with migmatites. The Cetmi, Karakaya and Denizgoren ophiolitic units all rest at the base of the upper plate, suggesting a possible reactivated obduction thrust as a precursor for the extensional detachments.

These detachment therefore superimpose resistant lithologies on top of HT metamorphic rocks, some other superimpose the same type of resistant units on top of weaker HP-bearing cover units as reviewed in the following.

In the Alpi Apuane, northern Italy, the Calcare Cavernoso mylonites (CalCa, table 1G, (Carmignani and Kligfield, 1990) are found between the upper Tuscan nappes made out of massive carbonates at the base and the subjacent blueschist-facies phyllites and metasandstones of the Massa and Autochtonous units. Localization of strain is due to intense cataclasis of anhydrite and dolostone along a reactivated thrust. The Liguride ophiolite on top of the whole lithotectonic pile has been preserved from most of the extensional tectonics.

In Corsica, the Tenda Shear Zone and the Balagne-Nebbio unit basal detachment constitute a multi-level detachment system (Jolivet et al., 1990; Marroni and Pandolfi, 2003) related to post-orogenic extension. In the Cap Corse antiform, the non-metamorphic ophiolitic Balagne nappe directly rests on the Schistes Lustrés calschists that preserved eclogite to blueschist facies assemblages. On the eastern edge of the Tenda massif, ophiolitic units and basement slices associated to the Schistes Lustrés are separated from the blueschist facies metagranitoids by a thick and complex mylonite zone developed to the expense of the latest.

All these examples therefore lie in intermediate position between the HT end-member or the HP preserving end-member and a theoretical third end-member, which would be represented by a detachment localized at the base of an anomalously strong upper plate.

Some other Mediterranean detachments also lie in intermediate position in the three end-member classification proposed here (Figure 5).

2.1.4 Detachments with intermediate characteristics

The Malaguides-Alpujarrides detachment (MAD, table 1A, Lonergan and Platt, 1995) in the Betics and the Naxos-Paros detachment (NaPaD, table 1Q, Gautier et al., 1993) in Central Cyclades plot along the HT and HP preserving members joint (Figure 5). Both indeed localized at the top of a HP bearing unit, and developed during a thermal reequilibration stage. This thermal reequilibration is more intense in the Naxos-Paros lower plate where prealpine basement underwent pervasive anatexis during exhumation (Vanderhaeghe, 2004), than in the Alpujarrides units, where high-pressure amphibolite facies overprint induced local migmatization in the top Herradura unit and pervasive resetting of radiochronometers (Azañón and Crespo-Blanc, 2000).

Other complex detachment systems such as the North Cycladic Detachment System in the Aegean (NCDS, table 1O, Jolivet et al., 2010a) or the Menderes detachments in Turkey also plot within the theoretical triangular classification, but show a singular evolution through time as detailed below.

2.2 Evolution of detachments through time

Three features identified in this review allow discussing how detachment systems evolve through time. When present, the nature of the collapse basin associated to extension along the detachment has been systematically noticed (Figure 6) and evidence how topography locally evolved during extension. The Cyclades and Menderes exhibit complex cases of multi-level detachment systems that evolved through time. Eventually relationship between ductile strain and brittle strain gives indices of how detachment systems behave when crossing the brittle-ductile transition.

2.2.1 Evolution of basins

Most of the syn-tectonic basins described in the hanging-walls of detachment systems have marine affinities or evolved through time from continental to shallow marine, suggesting a topography close to sea level, and most of the time subsiding during extension (Figure 6 and table 1, line 2.1). Accommodation is most of the time moderate, with shallow marine coarse facies, but turbidites are described in the Kazdag massif, suggesting a deep depositional environment (Bonev and Beccaletto, 2007). The opposite trend from marine to continental is only described on Naxos, where marine sandstones and pelites evolve into fluvial deposits (Bargnesi et al., 2013; Kuhlemann et al., 2004), implying that accommodation is decreasing with time, unless regional parameters actually prevail on local processes . Even in the case of detachments initiated in syn-orogenic conditions, such as in Crete, where possibly lacustrine breccias are described at the base of Neogene basins (Jolivet et al., 1996), no proper intra-montane collapse basins developed during activation of detachments in the Mediterranean realm. This implies that initial topography was close to or rapidly lowered to sea-level while MCC developed.

2.2.2 Evolution of strain localization

Complex detachment systems evolution can be traced in the three end-member classification proposed here. As for the Cyclades, the north-verging North Cycladic Detachment System (table 1O, Jolivet et al., 2010a) and south-verging Western Cycladic Detachment System (table 1R, Grasemann et al., 2011) are composed of several mylonite zones that successively localized strain during regional extension. In Northern Cyclades, the Tinos Detachment first localized along a former thrust at the top of the Cycladic Blueschist Unit and beneath the Upper Cycladic Nappe, constituted of a thick and resistant greenschist facies ophiolitic complex . Strain sequentially localized upward on the Livada detachment and then Mykonos detachment, while granites progressively intruded the lower plate and thermal reequilibration of the nappe pile occurred. On Mykonos, syn-tectonic granite directly roots in the highly strained migmatites of the lower plate (Denèle et al., 2011), evidencing a sharp contrast in thermal history between the upper and lower plates. In Ikaria, the Fanari ductile to brittle detachment located at the top of the syn-kinematic I type Raches granite and the ductile Agios Kyrkos shear zone show strain and age patterns similar to the North Cycladic Detachment System, and can be considered as the eastward extension of the same structure (Beaudoin et al., 2015; Laurent et al., 2015). The North Cycladic Detachment System therefore evolves from lower bound toward the HT end-member in the ternary classification proposed, with a perennial detachment zone relocalizing stepwise at the base of the upper plate while the lower plate exhumes. The Western Cycladic Detachment System described on

Kea, Kythnos and Serifos islands possibly followed the same evolution with initial detachment located at the base of the Pelagonian serpentinites and schists and progressively moving upward in the nappe pile as the thermal effect of syn-tectonic intrusions (on Serifos and Lavrion) modified the crustal rheological properties (Rabillard et al., 2015).

In Menderes, the initial structure that accommodated extension during Hellenic slab retreat is the Simav Detachment (SiD, table 1T, Isik and Tekeli, 2001). This large scale high strain zone is localized at the base of the Izmir - Ankara Ophiolite, within a HP nappes complex preserving eclogites and blueschists (Afyon, Tavsanli and Oren nappes (Plunder et al., 2013). Rocks in its footwall mainly consist of amphibolite facies gneiss with the metasedimentary Selimiye unit in uppermost position. Early northern Menderes granites are considered as syntectonic to SiD (Isik and Tekeli, 2001), due to development of high temperature foliation in these in the vicinity of SiD and overlap between their U-Pb zircon crystallization ages and cooling ages of biotites within derived mylonites (Dilek et al., 2009) in the early miocene . The younger Alasehir and Kucuk-Menderes Detachment systems, Central Menderes, Turkey (AlKuD, table 1T), subsequently cut across Menderes and divide it in Northern, Central and Southern domains. Rocks beneath and above the Alasehir and Buyuk Menderes detachments therefore derive from the same amphibolite facies metamorphic sequence (Bozkurt and Oberhänsli, 2001). The north-verging Alasehir detachment located at the top of the Salihli syn-tectonic granodiorite (Isık et al., 2003) in the late Miocene (Dilek et al., 2009) and the antithetic detachment at the base of the Buyuk Menderes graben also relates to the late Miocene intrusion of Menderes granites (Dilek et al., 2009). Even if recent migmatites are actually present within Menderes (Bozkurt, pers. comm.) the sole localization mechanism proposed so far for these detachments is the weakening due to granite intrusion. Strain indeed localized at the top of these plutons that evolve from isotropic in their core toward mylonites in the vicinity of detachment (Dilek et al., 2009). Mylonitic foliation is marked by biotites within granites and greenschist facies assemblages within mylonites. Strain therefore progressively localized during granite cooling and exhumation The central detachments accommodated the late stages of intra-Menderes extension in middle miocene times , while the top Menderes northern Simav detachment progressively ceased localizing strain (van Hinsbergen, 2010).

These complex long-life detachment systems systematically show an initial localization along intra-crustal rheological contrasts inherited from nappe stacking stages, the base of ophiolites and HP-bearing cover units being prone to such localization. The later stages are associated to HT metamorphism and/or syntectonic granite intrusions. Strain is then localized higher up in the tectonic pile (as in the Cyclades) on a structure synthetic to deeper precursors or symmetrically neoformed in the core of the already exhumed lower plate (as in Menderes).

2.2.3 Relationships with brittle deformation

When evidenced, relationships between brittle strain in the upper and lower plates and the ductile to brittle strain along the detachment system were systematically noticed (Table 1, items 2.4, and 4.3) . In most cases (Catena Costiera, Alpi Apuane, Rechnitz, Northern Cyclades, Northern Menderes) brittle strain is expressed as high- to low-angle normal faults, developed in the upper plate and rooting in the detachment zone. More rarely brittle deformation cuts across and offsets the main detachment system. When expressed as late stage high-angle normal faults (as in Balagne, Corsica, in the Motajica window, in southern and eastern Rhodope or Crete), this brittle strain can be viewed as late features accommodating the late stages of extension or unrelated later tectonics. The case of Elba island, with the development of the Zuccale fault, is a rare described case of a low angle brittle normal fault localizing independently of ductile inheritance and cutting across the extended nappe pile (Collettini and Holdsworth, 2004). This feature is also recognized today along the Apennine detachment system, with the low angle normal active Alto Tiberina fault cross-cutting all the thrust structures (Chiaraluce et al., 2007), which system the Zuccale fault zone also pertains to **(Collettini et al., 2006).**

Interpretation of relationships between ductile and brittle strain is not unique: depending on whether faults boarding basins are rooted on or cut across the detachment system, Menderes basin system can be viewed as syn-tectonic collapse structures (according to VanHinsbergen, 2010 for instance) or a wide rift zone with periodic rift basins oblitering the core complex structure (Ring et al., 2003).

2.3 Rheological implications of model end-members

The three end-members proposed in this review are not equally straightforward in terms of rheological implications. The HT end-member actually represents the most widely accepted definition of MCC, with a hot and hence low-viscosity lower crust. It has been quantitatively considered in many thermo-mechanical models (e.g. Rey et al., 2009; Tirel et al., 2006). A theoretical HS end-member with resistant upper crust, constituted of massive mafic or ultramafic lithologies thrust on top of a less resistant crust, can also be considered. Intra-crustal rheological contrast is here produced by the tectonic inversion of the rheological profile (Huet et al., 2010) and has been tested via thermo-mechanical modelling. The third HP end-member, representing detachments developing at the top or within HP cover units is less straightforward in terms of strength profile. Why would strain preferentially localize in or along such units in the post-thickening nappe pile ? (Huet et al., 2010) considered the Cycladic Blueschist Unit as a weak layer intercalated between the more resistant Upper Cycladic Unit ophiolite and the Cycladic Basement Unit constituted of granitoids mainly. Before testing the effect of such a layering, its relevance must be discussed. HP cover nappes can be considered weak due to the nature of their protolith. Initially constituted of shales and carbonates, they are fine grained, their water content is high and they are strongly foliated, thus being prone to localize deformation. Nevertheless, metamorphic transformations may significantly change their mechanical behaviour. In order to quantitatively discuss this point we performed thermochemical modelling of the impact of exhumation on average crustal lithologies (Figure 7). Modal evolution of a metabasalt, a metagranite and a metapelite with 10 wt% added water (dry compositions basalt and granite : Le Maitre (1976), shale : Boggs 1995) have been modeled with Theriak-Domino suite (de Capitani and Petrakakis, 2010) along different pressure-temperature paths from blueschist (1.2 GPa, 500°C) to lower greenschist facies (0.3 GPa, 200°C) using Holland & Powell database (Holland and Powell (2004) with Diener et al. (2007) activity model for amphiboles). Two cases can be considered : a path with thermal reequilibration coeval with decompression (path 1, Figure 7), and a path with decompression in the greenschist facies prior to substantial cooling (Path 2, Figure 7), more representative of the PT paths documented in HP units exhumed in Mediterranean MCC (Figure 3). In the case of a basalt, exhumation is marked by decrease in amphibole amount (due to glaucophane destabilization) whatever the path. Epidote is retrogressed into lawsonite along path 1 only. No substantial change in phyllosilicate content is observed whatever the considered path. In the case of a granite, the only substantial modal change modeled is a decrease then increase in phyllosilicate content along path 2. Eventually, in the case of a metapelite, epidote-lawsonite transition is also observed, and phyllosilicate content rises close to 50 vol% along path 2. Considering the amount of phyllosilicates as one of the first order mineralogical control on rocks strength in the blueschist/greenschist temperature range (Gueydan, 2004), the comparison of its evolution along paths for the different lithologies can yield the evolution of strength contrasts within a composite nappe pile (Figure 7D&H). As expected metapelites exhibit the highest phyllosilicates contents. No substantial contrast appear along path 1, while the more realistic two-stage PT path 2 exhibits a strong contrast between metapelites, reaching 40 vol. % phyllosilicates and other lithologies between 500 and 400°C i.e. within the ductile strain domain. It seems therefore that initially weak metasedimentary sequences are furthermore weakened by retrogression in the greenschist facies. Fluid transfers implied by these transformations also can lead to strength changes during exhumation.

HP cover units can therefore be considered at first order as weaker zones interlayered in the nappe pile, and therefore prone to localize deformation during syn-to post-orogenic extension. It seems from the presented review that the development of a perennial detachment during extension of a beforehand-thickened crust is therefore possible when a critical intra-crustal strength contrast appears, due to thermal reequilibration (HT MCC case) or due to inheritance (strong upper crust and weak middle crust). This conceptual model, can be quantitatively explored with thermo-mechanical models in order to estimate the order of magnitude of the required intra-crustal strength contrast and to assess how the different end-members can yield a detachment structure.

3. Numerical modelling

3.1 Numerical code used

The numerical code used in the present study is based on the FLAC algorithm (Cundall, 1989) and its subsequent evolutions (Burov and Poliakov, 2001; Poliakov et al., 1993; Yamato et al., 2007). Conservation of momentum equation and heat equation are iteratively solved. No radiogenic internal heating was implemented in the present simulations, mainly due to uncertainties on its value in the case of a crust resulting from complex nappe stacking. Thermomechanical coupling is enforced using Boussinesq approximation for the computation of density, including thermal stresses. Temperature is advected with the mesh within the Lagrangian formulation of the code. The rock behaviour is approximated by explicit visco-elasto-plastic rheology. Ductile deformation is modeled with a power-law and brittle deformation with a Mohr-Coulomb plastic flow law (table 3). The effective rheological behaviour is determined by current strain-rate, state of stress and temperature (Le Pourhiet et al., 2004). A marker-based remeshing procedure allows for handling of very large strains and displacements (Yamato et al., 2007). To focus on the influence of the rheological stratification, as in (Huet et al., 2010), the model setups have been deliberately simplified. Erosion, shear-heating, partial melting and mineral phase transitions are not considered in the computation.

3.1 Initial set-up and initial boundary conditions

Experimental design (Figure 8) directly derives from Huet et al. (2010). Thermal boundary conditions are 0°C at the surface and fixed initial temperatures at the bottom

(1000, 1200 and 1400 °C at 90 km, implying initial Moho temperatures between 398 and 1015°C, as listed in table 4). Lateral heat flow is set to zero. These thermal conditions allow to cover the complete crustal thermal gradient range (dashed curves on Figure 3) from low (13°C/km), as inferred from PT paths in the Cyclades for instance (Figure 3 and Huet et al., 2010) to moderate (18°C/km) as explored in previous thermo-mechanical modelling studies (Tirel et al., 2008 for instance).

Both sides of the models are assigned free slip condition. As in Huet et al., 2010, asymmetric lateral velocity is applied with 1 cm/yr on the lefthand side and 0 cm/yr on the righthand side.. Initial stretching rate for a 210 km long crustal segment is therefore 2.10^{-15} s^{-1}. This velocity boundary conditions corresponds to a mean value in the sensitivity tests to strain rates in numerical studies (Tirel et al., 2008), or in the velocity range used for analytical modeling (Buck, 1990). Upper surface is free, and bottom behaves as a Winkler foundation, ensuring local isostatic compensation (Burov and Poliakov, 2001). The initial velocity field is linearly interpolated from the boundary conditions and the stress is initially lithostatic and isotropic. No resistance or density anomaly is prescribed to localize strain, a random noise of 5 MPa has been instead added to the mean cohesion value (20 MPa, table 3) in the upper crust, except on a 20 km wide zone on the left hand side of the model where cohesion is set to 30 MPa in order to prevent artificial strain localization on the fast moving boundary (Huet et al., 2010).

The model is initially composed of a 210 km wide and 30, 45 or 60 km thick two-layers continental crust resting on top of lithospheric mantle. Initial mesh grid size is 0.75 x 1.25 km. All crustal layers have the same nominal density and thermal expansion coefficient (table 3), so that only temperature contrasts can yield density contrasts.

Mantle properties are the same in all simulations, its viscous behaviour is modelled as the one of dry dunite (Chopra and Paterson, 1984). Viscosity parameters for crustal layers derive from experimental data from quartz-diorite (Ranalli and Murphy (1987) as used in Tirel et al., 2008), dry quartzite (Ranalli and Murphy (1987) as used in Huet et al., 2011) and wet quartzite (Kirby and Kronenberg, 1987). Crustal structures can be rheologically homogeneous (27 simulations: d/d, q/q and w/w series in table 4) or heterogeneous. Among heterogeneous crust simulations,18 were performed with upper and lower crust the same thickness (evenly layered crust, table 4). 6 simulations were performed with total crustal thickness 45 km composed with quartz-diorite upper crust and dry quartzite lower crust, and 15 or 30 km thick upper crust.

3.2 Results

The 51 simulations run in this study are compared on the basis of the strain geometries produced by extension as well as P-T paths followed by the possibly exhumed lower crust. The different resulting geometries, exemplified in Figures 9, 10 and 11 are briefly described before a more statistical approach is proposed for all simulations. Only 3 cases out of 51 (X in table 4) yielded numerically unstable computation, with mantle rupturing from the very first stretching steps. These simulations, performed with cold conditions (bottom temperature 1000°C) are considered as geologically meaningless. Narrow rifts simulations all exhibit localized strain zones in the upper crust and upper mantle that connect across the ductile lower crust to stretch the complete crust to complete disruption after less than 10 Myr extension. They are characterized by high amplitude Moho deflection and limited lower crustal flow. Margin geometries produced exhibit complex geometries due to simple or complex rift systems (Figure 9C) isolating upper crustal blocks. Wide rift geometries (Figure 9B, D and F) show no transcrustal shear zones developing, upper crust disruption is compensated by lower crustal flow and Moho deflection is limited. Nevertheless, as analytically predicted by Buck (1991), lower crust resistance to flow is higher than plastic yield strength of the upper crust and strain relocalizes laterally, before an extended lower crust dome is formed. Strain localization shifts laterally in time with a wavelength determined by initial set-up. Metamorphic core complex geometries can be sub-divided into two sub-types : asymmetrical domes with a perennial detachment system assisting exhumation of the lower crust over the whole stretching event (Figure 10), and more symmetrical geometries with lower crust exhumation and strain localizing between two sub-domes (double-dome core complexes, Figure 11, DDCC in table 4). In both cases, the upper crust disruption is compensated by lateral and upward flow of the lower crust into a single perennial core. In the perennial detachment metamorphic core complex case (Figure 11, PDCC in table 4), strain relocalizes at the upper lower crust boundary yielding an asymmetric flow pattern in the lower crust and the persistence of a detachment system at the top of the dome structure with younging upward strain ages . The youngest rocks exhumed are then found beneath this detachment system, and exhibit "cool" PT path with no heating associated to decompression (Figure 10 B, F &G). In the double-dome core complex case (Figure 11) the high strain zone is located at the core of the exhumed lower crust, implying a symmetric flow pattern and exhumation ages younging from the edges to the core (Figure 11B & F). The later rocks exhume, the higher the amplitude of their decompressional heating (Figure 11G). Rocks exhumed within or close to detachments systematically show decompression paths along lower thermal gradients (Figures 10G & 11G). This remarkable feature is due to progressive cooling by the overriding upper unit, and might be less pronounced with viscous heating implemented in the code used. Thermal impact of viscous heating along extensional detachment systems has been estimated about 50°C temperature excess during decompression of hanging-wall units (Souche et al., 2013), and would therefore affect PT path shapes only on the second order.

Resulting geometries occur logically according to initial set-up (Figure 12). Narrow rifts are produced by thin crust simulations whatever their thermal state, except when lower crust is drastically weak. Wide rift geometry is indeed produced for wet quartzite lower crust simulation with initial crustal thickness 30 km and initial Moho temperature above 400°C (Figure 12C). On the other hand double-dome core complexes geometries are produced in thick crusts, whatever their thermal state, except when especially strong. Simulation with 60 km thick quartz-diorite homogeneous crust and TMoho =752°C indeed yield a wide rift pattern. The most sensible crustal thickness is 45 km. With this thickness, weakening of the whole crust promotes a switch from wide rift to double dome MCC pattern (Figure 12 A, B & C). Weakening of the lower crust only has the same effect but intermediate strength lower crust simulations (Figure 12D) yield wide-rift geometry when cold and perennial detachment MCCs pattern when warmer. The position of the intra-crustal strength contrast within the crust also has an impact. Thinner lower crust geometries (line 2/3 on Figure 12F) yield a narrow rift pattern when cold, which can be explained by an easier connection between localized strain in the upper crust and in the mantle and an overall less ductile rheology (higher ductile/brittle ratio). Thicker lower crust simulations (lower ductile/brittle ratio, line 1/3 on Figure 12F) yield more distributed extension mode (wide rift or double dome MCCs according to thermal state). Perennial detachment MCCs are produced for intermediate and maximal initial Moho temperatures and low to intermediate lower crust thicknesses. From this analysis, several general comments arise: i- thermal state is not the dominant controlling factor on extension modes, at least in the range explored here, ii- crustal thickness has a critical impact in the 30-60 km range, iii- perennial detachment MCCs are developed only in specific conditions with intermediate initial crustal thicknesses and intermediate intra-crustal strength contrasts.

In order to explain them with unified criteria, occurrences of the four final geometries described here (narrow and wide rifts and metamorphic cores with perennial detachment or double dome geometry) have systematically been reported against initial thermal and rheological parameters for the tested lithospheres (Table 4 and Figure 13). Intra-crustal strength contrast, i.e. ratio between the strength at the brittle-ductile transition depth and viscous strength of the crust at Moho depth as well as the integrated lithospheric strength expressed in MPa.km, have been calculated from the initial conditions of all models. These parameters have been chosen for their relevance, as well as for their easy calculation for already published comparable studies (cf discussion). Tested integrated strengths range over more than 1 order of magnitude, cold and thin crusts leading as expected to stronger lithospheres than warm and thick ones. Intra-crustal strength contrasts range over 4 orders of magnitudes, with the thin and cold crusts having contrast ratios lower than 10 and warm and thick crust exhibiting ratios higher than 10^4. Rift geometries are produced for high lithospheric strength and low strength ratios. Only such lithosphere can indeed reach their plastic yield strength and connect localized upper crust strain to localized strain in the mantle. Wide rift geometries are produced over a wide range of integrated strength but a narrow range of strength ratio. This reflects the close balance between upper crust strength and lower crust ability to flow implied by the development of wide rifts. Double dome MCCs are develop over a wide range of integrated strengths for strength ratios higher than 10^3. The specific conditions prone to the development of perennial detachment appear as a narrow intra-crustal strength contrast range close to 10^3. In this range, all the possible extension modes are actually produced; only rifts are produced for contrasts lower than $10^{2.5}$ (i.e. ~ 300) and only double dome MCCs are produced for contrasts higher the $10^{3.5}$ (i.e. ~ 3000).

The effect of each tested parameter can be precised with series having one varied parameter only (dashed lines on Figure 13). As expected, the initial crustal thickness and initial thermal state impact both parameters. Thick and/or warm crusts yield high intra-crustal strength contrast for low integrated strength. Layering has an impact on contrast more than on integrated strength. The intra-crustal strength contrast parameter is actually irrelevant to investigate the effect of the depth of inherited strength discontinuity within the crust (crosses on Figure 13). More sophisticated parameters would help, but would necessarily be more design-dependent.

The parametric study presented here yields some qualitative and quantitative conclusions about the boundary conditions and lithosphere properties prone to the development of MCC patterns. First, MCCs can form in moderately thickened crust along geotherms as low as 13°C/km. Depending mainly on the intrinsic strength ratio between the upper and lower crust, two types of MCCs can develop: double domes for crusts with a high strength ratio, MCCs with a perennial detachment at their top for crusts with a strength ration close to 10^3. Exhumed lower crust material shows limited heating during decompression in MCCs with a perennial detachment, and only material exhumed late in double-domes exhibits substantial heating. MCC pattern development is therefore thermally compatible with the preservation of HP-LT paragenesis in their core, especially on their limb.

4. Discussion

4.1 Parameter study and published MCC models : critical intra-crustal strength contrast for MCC formation

In order to test our parameter study against published analogue studies, the same parameters (intra-crustal strength contrast and integrated lithosperic strength) were computed for published simulations with comparable initial set-up (Figure 14). 32 simulations from Tirel et al. (2008) and 9 cases study in Huet et al (2011) were performed with the same numerical code as present and layered or homeogeneous crustal geometries. Among the 4 simulations presented in Rey et al. (2009) and performed with the Ellipsis finite element code (Moresi et al., 2003), the 2 melt-free cases with varied stretching rate (2.10^{-16} and 2.10^{-15} s^{-1}) can yield representative initial crustal strength constrast and integrated strength values. In the study performed by Schenker et al. (2012), with the I2VIS code (Gerya and Yuen, 2003) 12 initial geometries were tested with a rheologically homogeneous crust and varied initial thickness and Moho temperatures. In these two studies, partial melting is implemented as a viscosity drop down to a threshold value (10^{18} Pa.s in Rey et al., 2009, 10^{17} Pa.s in Schenker et al., 2012). Eventually, the two-layer wedge shape crust simulations without prescribed weak zone (A and B type models) from Wu et al. (2015), performed with a modified version of PARAVOZ (Tan et al., 2012) can be plotted on the same diagram as segments between their thin and thick ends. Compilation of these simulations with ours give a 108 simulations dataset, produced by different numerical codes, different crust and mantle representative materials, and a variety of boundary conditions. They all plot along the same trend in the intra-crustal strength contrast vs integrated lithosphere strength. Tirel et al. (2008) explored a linear domain across the whole possible field, while Huet et al. (2011) and Rey et al. (2009) focused on weak lithospheres and intermediate strength profiles. The equivalence between the present-study classification and other studies is not straightforward. The "double-domes" produced by Rey et al. (2009), the spreading domes in Huet et al., (2011) and the double-dome MCCs in the present study can be considered as equivalents. The "true rifts", "wide rifts" and "MCCs" produced in Huet et al. (2011) are respectively synonyms in terms of dynamics with rifts, wide rifts and perennial detachment MCCs produced here. Even if Schenker et al. (2012) mainly focused on the impact of the depth of the heat source (within the crust or within the mantle) on the lithospheric response, their classification also has a morphological basis. The "dysharmonic dome" and "lower crustal dome" types distinguished actually respectively correspond to the perennial detachment mode and the double-dome core complex types used here. "Gneiss domes" and "narrow rifts" structures produced in Wu et al. (2015) with 2 layer crusts show some periodicity that could relate them to wide rifts produced in the present study. In first approximation, "narrow rifts" and "continental margins" types can be considered as localized extension modes with crustal necking, while the "gneiss dome" mode compares with the double-dome MCCs produced here. In Tirel et al. (2008) the only available categorization is "crustal necking" vs "MCC". Even if presented examples of MCCs rather exhibit perennial detachment core complexes geometries, we keep the classification as simple as published. This compilation eventually shows that rifts or MCCs can be produced over a wide range of integrated lithospheric strength. Intra-crustal strength contrast seems a sensitive parameter for extension mode prediction: here again, only rifts are produced for contrasts lower than $10^{2.5}$ (i.e. ~ 300) and only double dome MCCs are produced for contrasts higher the $10^{3.5}$ (i.e. ~ 3000).

Tirel et al. (2008) extensively explored the effect of strain rate on extension mode, and Rey et al. (2009) also varied this parameter. Their results on this diagram show that an increase of 1 (for Rey et al., 2009) or close to 1 (for Tirel et al. ,2008) order of magnitude only slightly modifies the crustal properties, and only changes extension mode for lithospheres in the critical domain next to 10^3. Wu et al. (2015) who studied the effect of layered wedge shape come to the same conclusion as here: intrinsic strength contrast due to inherited layering is a first order parameter for changing extension mode. The realistic values used in that study actually cover a 2 orders of magnitude range in strength contrast between the strongest (plagioclase above dry quartz) and the weakest (plagioclase above wet quartz with 0.12 % added water).

Scaling of analogue models in Figure 14 diagram is impossible, but viscosity and strain rates values used in (Brun et al., 1994) allow the calculation of a $10^{1.2}$ intra-crustal strength contrast in the tilted-block mode extension and $10^{2.39}$ contrast in MCC mode. Here again, an increase about 1 order or magnitude is sufficient to promote MCC pattern development.

Since the first order parameter often considered as critical for MCC pattern development is initial thermal state (Buck, 1991, Tirel et al., 2008) to such an extent that MCCs are sometimes considered as restricted to warm lithospheres, the effect of intra-crustal strength contrast can be evaluated in regard to initial Moho temperature (Figure 15). All simulations considered here cover a wide domain of initial thermal conditions between 400°C and 1340°C Moho temperatures, i.e. much wider that the expected possible values, even in the most severe post-orogenic thermal relaxation. The present study produces MCCs with initial Moho temperature as cold as 680°C. Huet et al. (2009) and Wu et al. (2015) yielded the same result, highlighting that cold MCCs constitute a thermo-mechanically sound concept. The rift patterns with the initially warmest lithosphere were actually produced by Tirel et l. (2008). The domain in which the different models can give any of the distinguished extension modes actually span from 470°C to 950°C initial Moho temperature, meaning that thermal state, in its admitted range, is not a critical parameter for predicting lithospherical extension mode.

4.2 Numerical insights versus Mediterranean examples

4.2.1 Natural vs numerical categorization

The parametric study presented here, together with a compilation of similar numerical modelling of continental extension modes leads on one hand to a 4 end-member model, with double domes MCCs, perennial detachment MCCs, wide rift and narrow rift as possible resulting geometries. On the other hand, the review of Mediterranean extensional MCCS points to a 3 end-member categorization of MCCs : HT MCCs with a high temperature lower unit, HP MMCs with an interlayered high-pressure nappe preserved in the vicinity of the detachment, and High Strength (HS) upper crust MCCs localizing strain at its base. The juxtaposition of both reviews enables discussing the mechanical properties behind the three natural types defined here. Actually each of the numerical studies also explored a ternary diagram with 3 end-members : high temperature, weak middle crust and strong upper crust (Figure 15 inset) that resembles the ternary diagram used for classification of natural meditarranean cases. Weak middle crust relate to the HP natural end-member, and strong upper crust to HS end-member. Tirel et al. (2008), Schenker et al. (2012) as well as the high temperature experiments conducted here confirm the acknowledged behaviour of continental lithosphere with high thermal gradient (HT end-member). Within this category the distinction of double-dome vs perennial detachment MCCS will de discussed further. Huet et al. (2009) explored the effect of an inter-layered weak zone, representing a HP metasedimentary nappe in natural cases. In this respect, they explored the left joint of the ternary diagram. The present study, with 2-layer crust lithospheres, as well as Wu et al. (2015) *pro parte* explored the right-hand joint of the diagram. Numerical modelling therefore evidences the mechanical feasability of all natural end-members.

4.2.2 Natural double domes and perennial detachment MCCs in nature

Not all natural cases can be plotted in the diagram derived from numerical simulations (Figure 16), since their initiation thermal conditions and intra-crustal strength contrasts remain uneasy to assess. Nevertheless, some of them can be qualitatively localized and tend to confirm the relevance of this categorization. The description of double-domes by Rey et al. (2009) is based on a two dimensional projection of Naxos core complex main features. Schenker et al. (2012) also consider Naxos as a natural case for their collisional heat induced migmatitic core complex, while Rhodope represents the asthenospheric heat induced migmatitic core complex. These cases (table 1) all illustrate the high temperature-high strength(Figure 16) end of our simulations, with low-viscosity migmatites exhumed in the core of the lower plate beneath a detachment located at the base of an unmetamorphosed ophiolite-bearing unit. Among cold MCCs, the Catena Costiera detachment (Rossetti et al., 2004) exhumed blueschist continental metaclastics and marbles beneath a greenschist ophiolitic melange. Mylonites and cataclasites derived from weak marbles and metapelites, implying a strong inheritance effect. Strain indicators show a pervasive asymmetric sense of shear toward NNW, related to the activation of a single detachment zone. Other large MCCs such as Northern Cyclades, Motajica, Menderes or Betic cordilleras actually show evolution through time that can relate to the evolution of the mechanical properties of the crust they develop in.

Compilation of PT paths in metamorphic units from the Aegean domain {Jolivet:2008eb} shows variations in decompression paths similar to synthetic paths computed from numerical modelling (Figures 10G & 11G), with cooler paths for the latest rocks exhumed in Crete or in Peloponnese. PT paths shapes are therefore relevantly reproduced without viscous heating in our models testifying that this process is a second order phenomenon in detachment system, especially when weak lithologies are implied over time scales about 10 Myr (Souche et al., 2013) or that shear heating is counterbalanced by local cooling processes such as fluid advection within detachment (Famin et al., 2004, Mezri et al., 2015).

4.2.3 Temporal evolution of multiple detachment systems

Detachment systems (§ 2.2.2) as well as smaller structures with several detachments (Betics and Motajica for instance) can be described as a sequence of changes in strain localization levels. Menderes and Cycladic systems evolve toward the high temperature end-member in the ternary diagram proposed for natural cases (Figure 5). Nevertheless, their mechanical evolution differ and they do not follow the same trend in the intra-crustal strength contrast vs thermal state diagram (Figure 16). In Menderes (Figure 17A), strain is first localized at the base of or within the high-pressure metamorphic rocks and the Izmir Ankara Ophiolite, along the Simav Detachment, which actually reactivates an older thrust. Whether the equivalent thrust at the base of the Lycian nappes effectively accommodated extension remains unknown. Even though the intrusion of the syn-tectonic Egrigoz granite (crystallization at 20-21 Ma and cooling at 20 Ma, Dilek, 2009) is expected to lower the effective strength of the detachment zone, mylonites along Simav Detachment exhibit similar ages (22.8 Ma, Tekeli, 2001) implying a short activation duration for the Simav Detachment. Strain is accommodated in a second time within the lower plate, between 16 and 7 Ma according to syntectonic granites ages (Figure 17A), basin infills in hanging-walls of detachments (16.7 to 14.9 Ma) and dating of white micas in mylonites (7 ± 1 Ma Lips, 2001). The Alasehir and Buyuk detachments (Table 1) constitute a synchronous and antithetic detachment pair, that relocates strain at the core of the Menderes massif while stretching goes on. This implies that this domain is eventually weaker than the previously activated Simav Detachment zone, probably due to crustal thinning, rise of thermal state and intrusion of granites. Intra-crustal strength contrast is probably rising with thermal state during stretching and extension mode evolves from perennial asymmetric detachment to a double-dome symmetric MCC.

In Northern Cyclades (Figure 17B) the successive Tinos, Livada and Mykonos detachment zones (Jolivet et al., 2010) progressively relocate strain higher within the upper plate while stretching develops from 30 to 9 Ma and thermal state increases with consecutive intrusions of syn-tectonic granites at 14-15 and 11-13 Ma. Late reactivation of the Vari detachment on Syros at 10 Ma is limited and the North Cycladic Detachment System can be considered as a perennial asymmetric detachment system responsible for most of the exhumation in northern Cyclades. It seems that intra-crustal strength contrast remained governed by inheritance and that intrusion of granites only promoted upward migration of the shear zone within the upper plate. For this reason, the North

Cycladic Detachment System evolution can be viewed as a rise in thermal gradient without drastic change in intra-crustal contrast through time.

The Betic cordilleras (Figure 17C) clearly show a double detachment system, with the older Malaguides-Alpujarrides Detachment (activated from 23 to 20 Ma) on top and the younger Mecina-Filabres Shear Zone (activated from 16 to 7 Ma, Augier et al, 2005). While the first one is highly asymmetric with only top-to-the-North shear sense indicators developed in the northern mylonitic edge of the Sierra de las Estancias massif (Lonergan and Platt, 1995), the Mecina Filabres shear zone wraps a multiple dome structure (Sierra de los Filabres and Sierra Alhamilla) with divergent shear sense indicators (Augier et al., 2005a). Even if highly tridimensional, this pattern implies that the older detachment system (MAD, Figure 17C) progressively hardens while lower detachment activates.

In the Carpathian (Figure 17D), the Motajica dome is also the result of a two stage extension between 25 and 13 Ma (Ustaszewski et al., 2010). Until 18 Ma, the main structure accommodating strain is the former Tisza-Dacia unit basal thrust reactivated as a detachment, strain is then accommodated along a symmetric listric faults system (Figure 17D) that cuts across the Motajica Detachment. The Motajica granite, that yielded a 27 Ma U-Pb zircon age (Ustaszewski et al., 2010) predates the regional extension stage so that relocalization of strain within the metamorphic Sava zone cannot be ascribed to intrusion. Nevertheless, this example is a supplemental illustration of the recurrent evolution from perennial detachment MCCs toward double-dome MCCs with increasing stretching of the crust. This conclusion is apparently opposite to the temporal evolution of extension modes speculated from short term modelling (Buck, 1991) and exemplified by the Basin and Range: from MCC to wide-rift and then narrow-rift. Ring et al. (2003) also view Menderes as a wide-rift structure overprinting a former MCC pattern. The main difference between these two evolutions is the heat budget and time scale. The perennial detachment toward double-dome MCC evolution implies heat input at the base of the crust higher than heat dissipation due to stretching, due to lithospheric stretching for instance, while the MCC toward rift evolution implies a decreasing heat budget due to efficient heat dissipation during MCC extension phase. While the first evolution seems supported by natural evidences over short time periods (15 to 20 Myrs in examples developed here, Figure 17), the later could be relevant for longer time-scale evolutions (over more than 40 Myrs for the Great Basin MCC cluster (Dickinson, 2002)

4.3 Thermal state, inheritance, strain rate and metamorphism as controlling parameters for intra-crustal strength contrast

The present study after other numerical modelling of extension modes of the continental lithosphere (Huet et al., 2010; 2011; Rey et al., 2009; 2011; Tirel et al., 2008; 2006; Wu et al., 2015) enables to discuss the balance between parameters controlling the intra-crustal strength contrast within the crust. The present compilation of models shows that an exaggeration of one order of magnitude of the intra-crustal strength contrast is sufficient to switch extension mode from rifting to MCC. In a crude approximation, the impact of the different parameters invoked is to lower the effective strength of the lower crust. Maximum strength within the crust being controlled by frictional behaviour, it is unlikely to vary over one order of magnitude for material governed by Byerlee's law. Using the different lithologies considered as relevant for crustal materials (diorite, quartzite and wet quartzite), a simple calculation of effective strength for various temperatures and strain rates (Figure 18) shows that for a quartz-diorite at 650°C, strained at $10^{-13.5}$ s^{-1}, strain rate must decrease of more than 2 orders of magnitude (A in Figure 18), or temperature must rise of 200°C (B in Figure 18) to lower its effective strength of 1 order of magnitude. Alternatively, a wet quartzite in the same conditions is also 10 times less resistant (C in Figure 18). Strain rate and temperature therefore must change drastically in order to promote high intra-crustal strength contrast. Layering due to inheritance can therefore be a first order parameter responsible for such contrasts. These three effects actually can add up: a warm and layered crust stretched at a low strain rate will definitely develop a MCC pattern.

Together with layering, inner complex structures can be inherited from preliminary thickening stages. Dipping lithological contrast have a strong impact on extensional behavior of the crust (Huet et al., 2011; Le Pourhiet et al., 2004; Wu et al., 2015). Lateral strength contrast gradients produced with realistic geometries (Wu et al., 2015) are also about 1 order of magnitude (Figure 14). Dipping interfaces therefore also constitute a first order inheritance effect. Transcurrent structures, prone to develop during thickening

Metamorphic reactions responsible for destabilization or crystallization of weak phases or fluid influx were not taken into account in all the studies considered here, that all focused on materials with continuous rheology. According to experimental studies (Jaoul et al., 1984), a quartz aggregate with 0.28 wt% H_2O has an effective viscosity 100 times lower than a dry aggregate. This severe effect implies that the destabilization or crystallisation of a limited percentage of hydroxyl-bearing minerals during the exhumation of the lower plate (Figure 7) can induce high intra-crustal strength contrast. This effect has also been implemented in numerical modelling with complex feedback between strain, permeability and metamorphic reactions (Mezri et al., 2015). It appears that models implementing water-controlled phase change develop an asymmetric detachment MCC evolving into a double-dome MCC, while reference model (TMoho 810°C, stretching rate 0.8 cm/yr) yields a narrow rift extension pattern. Second invariant of strain rate tensor in the high fluid flux domains is more than one order of magnitude higher than in the low fluid flux domains, implying a weakening effect of more than one order of magnitude. Partial melting, observed in most of high temperature MCCs cores, has also been considered in models as a sharp viscosity drop within the lower crust (Rey et al., 2009, Schenker et al., 2012). When implemented as such, solidus envelope at depth constitutes a sharp intra-crustal strength contrast and promotes the development of double-dome MCCs. Intra-crustal strength contrasts in these cases are close to 3 orders of magnitude higher than the critical value defined here (Figure 14, 15).

Conclusion

The understanding of MCC development and the localization of strain on a perennial detachment zone was initially based on models with homogeneous crust, and highlighted the major role of crustal thickness and temperature in the mode of extension of continental lithosphere. The examination of natural cases in the Mediterranean realm emphasizes a second type of MCCs exhuming "cold" metamorphic rocks beneath a detachment system localized along sharp intra-crustal strength contrast inherited from thickening stages of orogenic crusts. Interlayered HP parametamorphic nappes and basal contacts of resistant upper units most of the time localize extensional strain. The comparison of new and published numerical models of extending continental lithosphere confirms the mechanical feasability of core-complex in continental lithosphere with low thermal gradients and marked layering. It also shows that intra-crustal strength contrast is a key parameter for predicting the extension mode of continental lithosphere. Beyond a critical value of 1000, MCCs develop, whatever the initial thermal state, thickness or strain rate. For high values of this contrast, double-dome core complex develop, with strain progressively re-localizing at the center of the footwall during stretching, while asymmetric dome geometries with one perennial detachment are produced for intra-crustal strength contrast close to 1000. Natural examples of Mediterranean detachment systems also show these two MCC types, and evolution of multiple detachments system show that in most cases inheritance controls the first extension steps and asymmetric strain pattern, and that further stretching is accommodated by double dome dynamics, driven by thermal effects mainly.

The present study is based on mediterranean that share a common tectonic setting and possibly some specificities of the post-variscan crust and alpine cover. Nevertheless the proposed critical parameter for MCC development proposed here, i. e. the intra-crustal strength contrast and the gradation of extension modes and core-complex types could be used in comparable settings. The Cordilleran Core Complexes developed during post-orgenic extension or the numerous comparable studies recently described in China (Whitney et al., 2013) could also be considered in a broader review.

Acknowledgement

This study was initiated during the ANR EGEO project (PI L. Jolivet). This work has received funding from the European Research Council (ERC) under the seventh

Framework Programme of the European Union (ERC Advanced Grant, grant agreement No 290864, RHEOLITH). Authors thank C. Doglioni, editor, M. Barchi, reviewer and an anonymous reviewer for their constructive reviews and carefull handling of the present manuscript.

Table and Figure captions

Table 1 : Caracteristic features of Mediterranean detachments and associated domes and basins. Pand T estimates for metamorphic peak conditions (4.2) are given in supplemental table A1. A: amphibolite, BS: blueschist, E: eclogite; GS: greenschist, HANF: high angle normal fault, HPA: high pressure amphibolite, HPG: high pressure granulite, LANF: low angle normal fault, LPA: low pressure amphibolite,

Table 2 : Main features of Mediterranean detachments tectonostratigraphies. C for calc-mylonites, m/c for marine vs continental basins, S and P for syn- and post-orogenic initiations. c continental, m marine, off off-shore. The relative weighing of ticks between lines 1,2 and 3, line 4 and line 5 was used to place natural cases on figure 5.

AA Alpi Apuane, ABMDS Alasehir-Buyuk Menderes Detachment System, Asp Aspromonte, ASZ Alakeci Shear Zone, Bal Balagne basal contact, BB Beni Bousera, CaD Capanne Detachment, CCD Calcare Cavernoso Detachment, CMe Central Menderes, CR Corinth Rift, CrD Cretan Detachment, Ed Edough, GK Grande Kabylie, Ik Ikaria, Kaz Kazdağ, KD Kabylian Detachment, KnD Kerdylion Detachment, LL Lubenik Line, MAD Malguides-Alpujarrides Detachment, MeSZ Messaria Shear Zone, MFSZ Mecina-Filabres Shear Zone, Mo Motajica, NCDS Northern Cycladic Detachment System, NCy Northern Cyclades, Ni Niğde, NP Naxos-Paros, NPD Naxos Paros Detachment, SD Simav Detachment, SD Simav Detachment, Sy Syros, Sif Sifnos, TeSZ Tenda Shear Zone, TKD Tokachka-Kesebir Detachment, VD Vari Detachment,Ve Veporic, ZFZ Zaouia Fault Zone.

Table 3 : Rheological parameters used and varied for the differents models. Dislocation creep law for the mantle is dry dunite (Chopra and Paterson, 1984), and for the crust quartz-diorite and dry quartzite (Ranalli and Murphy, 1987) and wet quartzite (Kirby and Kronenberg, 1987).

Table 4 : Simulation results. Each simulation is named after its layering (d: quartz-diorite, q: quartzite, w: wet quartzite), the initial crust thickness, in km, and initial bottom temperature in Celsius. Evenly layered crusts have two half-crust layers. All parameters are computed with initial geometry and a 1 $cm.yr^{-1}$ stretching rate for a 210 km long crustal segment, i.e. strain rate = 2.10^{-15} s^{-1}. Intra-crustal strength contrast is the ratio of maximum strength at the brittle-ductile transition over viscous strength at Moho depth, Integrated lithospheric strength is calculated on the 90 km height of models. Result types are listed as : R, narrow rifts, WR, wide rifts, PDC perennial detachment core complexes, DDC double dome core complexes. X refers to geologically meaningless simulations. Bold lines refer to simulations used as examples in figures 8, 9 and 10.

Figure 1 : Principle sketch of a Metamorphic Core Complex, showing the association of structures and fault-rock types considered as symptomatic for ductile extensional mode. Rheological envelope associated to these structures is also shown. BDT : Brittle-ductile transition.

Figure 2 : Map of Mediterranean core complexes on top of Moho isobaths, homogenized and smoothed after (Dèzes and Ziegler, 2001; Di Luccio and Pasyanos, 2007; Koulakov and Sobolev, 2006; Marone et al., 2003; Tiberi et al., 2001) The large Menderes and Betics domes have been subdivided into units. Shoreline in white.

Figure 3 : Pressure temperature conditions estimated for Mediterranean detachment footwalls compared to initial Moho temperatures ascribed in numerical models for MCC formation. Curves 1 : wet solidus of granite (Huang & Wyllie, 1981), 2 and 3 are maximum and minimum initial thermal gradients tested in the present parametric study.. AA Alpi Apuane (1 Mass, 2 Autochthon), Alpu Alpujarrides (1 Herradura u., 2 Sadobreña & Adra u. 3 Escalate u., 4 Lujar Gador u.), And Andros, Asp Aspromonte, BB Beni Bousera (1 mafic rocks, 2 kinzigites, 3 Filali schists), CC Catena Costiera, Ed Edough, ERho Eastern Rhodope (1 HP peak, 2 HT,), GK Greater Kabylie (1 Sidi Ali Bou Nab u., 2 migmatites), Ik Ikaria,, Kaz Kazdag, Me Menderes (1 Cine u. HP , 2 Cine u. HT - 3 Bozdag u., 4 Selimye u.), Mot Motajica, Nax Naxos (1 HP, 2 HT)NF Nevado-Filabrides (1 Bedar Macael u. , 3 Phase D3), Ni Nigde, , Re Rechnitz (1 & 2) SRho Southern Rhodope (Thasos), Sy Syros (1 high pressure, 2 late overprint) Eclogite peak 2 GS retrogression), Te Tenda massif, Corsica, Tin Tinos (1 Eclogite peak, 2 BS stage, 3 transition, 4 GS retrogression), Ve Veporic.

P,T values and references are given in supplemental material table A1

Figure 4 : Tectonostratigraphic positions of Mediterranean detachments. Colors refer to metamorphic facies: pale yellow, undisctinct low grade, green: GS greenschist, orange: A amphibolite, brown: G granulite, blue: BS blueschist, purple: E, eclogite. Relevant lithologies are precised. Extensional detachments are abbreviated as in Table 1.

Adria. Adriatic plate, Alpu. Alpujarrides, Aspro. Aspromonte u., APU Amphibolites-Peridotites u., BMD Buyuk Menderes detachment, CBS Cycladic Blueschists, Eg Egrigoz granodiorite, FD Fanari Detachment, Ghom. Ghomarides, GT Gavrovo Tripolitza, Gum.

Gumusler, HGMU High grade metasedimentary u., HPU High pressure u., IAO Izmir-Ankara ophiolite, LANF Low Angle Normal Fault, LiD Livada detachment, Malag. Malaguides, MGU Migmatite-granite u., Mul Mulhacen, MyD Mykonos detachment, N.F. Nevado-Filabrides, NMM, CMM & SMM North Central and South Menderes massifs, Pelag. Pelagonian, Phyllites-Q. Phyllites-quartzites, Pi Pindos, Ro Rochovce, S. L. Schistes Lustrés, Seb. Sebtides, TB Tyros beds, Tell. Tellian u., TiD Tinos Detachment, Tu Turgutlu granite, UOU, LOU Upper and Lower ophiolite u., ZF Zaroukla fault

Figure 5 : Ternary diagram representing the balance of thermal and inheritance effects on the different Mediterranean extensional detachments, abbreviated as in Table 1. Positions in the triangle come from the relative weighting of caracteristic features listed in table 1. Regular case : detachments inherited from syn-orogenic tectonics, bold case : post-orogenic detachments. HT high temperature footwall, HP high pressure unit preserved in the footwall, HS high strength hanging wall. White arrows represent time evolution of detachment systems.

Figure 6 : Synoptic comparative time evolution or relative position of syn-detachment collapse basins preserved in the Mediterranean realm according to their sedimenrary infill. Arrow senses represent time evolution : most of basins evolve tward marine (downward arrows), only NaPaD basin is evolving from marine to continental with time (upward bold arrow). Color represent paleobathymetry for marine basins (light grey: shallow, darker grey: deep) Refers to line 2.1 in table 1 and references therein. Abbreviations as in table 1.

Figure 7 : Thermochemical modelling of mode evolution of three protoliths representative for pelites, granites and basalts as detailed in table I B95, Boggs, 1995, LM76 : Le Maitre, 1976. A, B, C and E,F,G : modal evolutions in volume fractions along

paths 1 and 2 as shown on J. Micas are phengite and paragonite together. More chaotic curves in C and G are due to poorly constrained complex local equilibria along main reactions in mafic rocks. D and H : Phyllosilicates volume fraction evolution along the same paths. Shaded areas represent brittle quartz domain.

Figure 8 : Set-up of numerical experiments initial conditions for a 45 km thick double layered crust (?/?_45_???? cases in table 4) See Huet et al., 2011 for details. Bottom temperatures are varied between 1000, 1200 and 1400°C. Resulting initial Moho temperatures are listed in table 3. Hatched column on the left represent a 20 km wide area with no noise on cohesion and a higher cohesion (30 MPa instead of 20 MPa).

Figure 9 : Compared output of numerical experiments for simulation d/q_30_1400, representative of a rift-type extension mode (A & C) after 6 Myr stretching and simulation q/q_45_1200 representative for the wide rift extension mode after 12 Myr stretching. White curves show foliation trajectories from finite strain computed as in Huet et al., 2011. C & D represent instantaneous strain rates. Initial strength profiles computed for 2.10^{-15} s^{-1} and parameters detailed in table 2 are depicted in E and F. Values are precised in table 3.

Figure 10 : Simulation d/q_45_1200 output representative for perennial detachment core complex extension mode. A & B : geometry after 4 and 14 Myr stretching, with position of markers used for PT and exhumation calculations. White curves show foliation trajectories from finite strain computed as in Huet et al., 2011. C & D : instantaneous strain rates profiles, E Initial strength profile computed for 2.10^{-15} s^{-1} and parameters detailed in table 2F & G: exhumation history and PT paths for markers 1, 2 and 3.

Figure 11 : Simulation d/w_45_1200 output representative for double dome core complex extension mode. A & B: geometry after 4 and 14.1 Myr stretching, with position of markers used for PT and exhumation calculations. White curves show foliation trajectories from finite strain computed as in Huet et al., 2011. C & D : instantaneous strain rates profiles, E Initial strength profile computed for 2.10^{-15} s^{-1} and parameters detailed in table 2F & D: exhumation history and PT paths for markers 1, 2 and 3.

Figure 12 : Resulting geometries of the simulations run in this study. Series are refered to as in table 3. A, B & C represent homogeneous crust simulations, D and E evenly layered crust simulations and F unevenly layered simulations. Line 45 km on D represents the same simulations as line 1/2 on F.

Figure 13 : Intra-crustal strength contrast vs integrated lithosphere strength logarithm plot for all 48 meaningfull simulations listed in table 3. Effect of different tested parameters is highlighted by series tied by dash lines. Triangles: series d/q_X_1000, squares: series d/d_60_X, diamonds: d/X_45_1200, crosses: d/q_45_1200. 1/3, 1/2, 2/3 refer to the relative size of the upper crust in unevenly layered crust simulations.

Figure 14 : Intra-crustal strength contrast vs integrated lithosphere strength log-log plot for 46 published numerical simulations compared to present study. TS This Study, H11 (Huet et al., 2011), all 9 simulations are reported, T08 (Tirel et al., 2008) all 32 simulations reported, R09 (Rey et al., 2009) 2 simulations reported, with no melt effect at slow (2.10^{-16} s^{-1}) and fast (2.10^{-15} s^{-1}) stretching rate. S12 (Schenker et al., 2012) all 12 models reported. W15 (Wu et al., 2015) 3 models reported, with wedge-shape layered crust and no prescribed weak interface. Calculations were made at each initial model end (thick and thin ends). Bold squares : stretching rate effect, as explored by Tirel et al.

(2008) on the series with initial crustal thickness 60 km and initial Moho temperature 830°C (mantle heat flux 30mW.m^{-2})

Figure 15 : Intra-crustal strength contrast vs initial Moho temperature logarithm plot for 46 published numerical simulations compared to present study. Legend as in figure 14. Triangle inset refers to ternary end-member MCC types analogue to ternary diagram used for Mediterranean examples (Figure 5). Symbols at triangle edges refer to where different studies plot in this diagram.

Figure 16 : Synthetic diagramm showing preponderance of intra-crustal strength contrast over thermal state of the crust on extension mode in mediterranean natural cases on the basis of thermal evolutions recorded.

Figure 17 : Examples of time evolution of multiple detachment systems in the Mediterranean. Detachment named as in Table 1. Moho depth as in Figure 2. A Menderes, IAO : Izmir Ankara Ophiolite, modified after VanHinsbergen, 2010 and Ring, 2003, B- North Cycladic Detachment System, after Jolivet et al., (2010), C Betic Cordilleras after Augier et al. (2005) and Lonergan and Platt (1995), D Motajica after Ustazjewski et al. (2010). g. for granite

Figure 18 : Strength contours in MPa (presented with a logarithmic scale) for different crustal lithologies used in the present study. A, B and C are responsible for the same strength drop of 1 order of magnitude. A: strain rate drop, B: temperature increase, C: lithological change from quartz-diorite to wet quartzite.

References

Augier, R., Agard, P., Monié, P., and Jolivet, L., 2005, Exhumation, doming and slab retreat in the Betic Cordillera (SE Spain): in situ40Ar/39Ar ages and P–T–d–t paths for the Nevado-Filabride complex: Journal of Metamorphic Geology,, doi: 10.1111/j.1525-1314.2005.00581.x.

Augier, R., Jolivet, L., Robin, C., 2005b. Late Orogenic doming in the eastern Betic Cordilleras: Final exhumation of the Nevado-Filabride complex and its relation to basin genesis. Tectonics 24, n/a–n/a. doi:10.1029/2004TC001687

Avigad, D., 1998, High-pressure metamorphism and cooling on SE Naxos (Cyclades, Greece): European Journal of Mineralogy, v. 10, no. 6, p. 1309–1319.

Azañón, J.M., and Crespo-Blanc, A., 2000, Exhumation during a continental collision inferred from the tectonometamorphic evolution of the Alpujarride Complex in the central Betics (Alboran Domain, SE Spain): Tectonics,, doi: 10.1029/2000TC900005.

Bargnesi, E.A., Stockli, D.F., Mancktelow, N., and Soukis, K., 2013, Miocene core complex development and coeval supradetachment basin evolution of Paros, Greece, insights from (U–Th)/He thermochronometry: Tectonophysics, v. 595-596, p. 165–182, doi: 10.1016/j.tecto.2012.07.015.

Beaudoin, A., Augier, R., Laurent, V., Jolivet, L., Lahfid, A., Bosse, V., Arbaret, L., Rabillard, A., Menant, A., 2015. The Ikaria high-temperature Metamorphic Core Complex (Cyclades, Greece): Geometry, kinematics and thermal structure. Journal of Geodynamics 92, 18–41. doi:10.1016/j.jog.2015.09.004

Beccaletto, L., and Steiner, C., 2005, Evidence of two-stage extensional tectonics from the northern edge of the Edremit Graben, NW Turkey: Geodinamica Acta, v. 18, no. 3-4, p. 283–297, doi: 10.3166/ga.18.283-297.

Beccaluva, L., Bianchini, G., and Siena, F., 2004, Tertiary-Quaternary volcanism and tectono-magmatic evolution in Italy: Special Volume of the Italian Geological Society for the IGC 32 - Florence.

Block, L., Royden, L.H., 2010. Core complex geometries and regional scale flow in the lower crust. Tectonics 9, 557–567. doi:10.1029/TC009i004p00557

Bonardi, G., Cavazza, W., Perrone, V., Rossi, S., 2001. Calabria-Peloritani terrane and northern Ionian Sea, in: Anatomy of an Orogen: the Apennines and Adjacent Mediterranean Basins. Springer Netherlands, Dordrecht, pp. 287–306. doi:10.1007/978-94-015-9829-3_17

Bonardi, G., Giunta, G., Perrone, V., Russo, M., Zuppetta, A., and Ciampo, G., 1980, Osservazioni sull'evoluzione dell'arco Calabro-Peloritano nel Miocene inferiore; la formazione di Stilo-Capo d'Orlando: Bollettino della Societa Geologica Italiana, v. 99, no. 4, p. 365–393.

Bonev, N., Beccaletto, L., 2007. From syn- to post-orogenic Tertiary extension in the north Aegean region: constraints on the kinematics in the eastern Rhodope Thrace, Bulgaria Greece and the Biga Peninsula, NW Turkey. Geological Society, London, Special Publications 291, 113–142. doi:10.1144/SP291.6

Bonev, N., Burg, J.P., Ivanov, Z., 2006. Mesozoic–Tertiary structural evolution of an extensional gneiss dome—the Kesebir–Kardamos dome, eastern Rhodope (Bulgaria–Greece). Int J Earth Sci. doi:10.1007/s00531-005-0025-y

Bonneau, M., 1984, Correlation of the Hellenic nappes in the south-east Aegean and their tectonic reconstruction: Geological Society, London, Special Publications, v. 17, no. 1, p. 517–527, doi: 10.1144/gsl.sp.1984.017.01.38.

Bosch, D., Hammor, D., Mechati, M., Fernandez, L., Bruguier, O., Caby, R., Verdoux, P., 2014. Geochemical study (major, trace elements and Pb–Sr–Nd isotopes) of mantle material obducted onto the North African margin (Edough Massif, North Eastern Algeria): Tethys fragments or lost remnants of the Liguro–Provençal basin? Tectonophysics 626, 53–68. doi:10.1016/j.tecto.2014.03.031

Bozkurt, E., Oberhansli, R., 2001. Menderes Massif (Western Turkey): structural, metamorphic and magmatic evolution - a synthesis. Int J Earth Sci 89, 679–708. doi:10.1007/s005310000173

Bruguier, O., Hammor, D., Bosch, D., Caby, R., 2009. Miocene incorporation of peridotite into the Hercynian basement of the Maghrebides (Edough massif, NE Algeria): Implications for the geodynamic evolution of the Western Mediterranean. Chemical Geology 261, 172–184. doi:10.1016/j.chemgeo.2008.11.016

Brun, J.-P., and Sokoutis, D., 2007, Kinematics of the Southern Rhodope Core Complex (North Greece): International Journal of Earth Sciences, v. 96, no. 6, p. 1079–1099, doi: 10.1007/s00531-007-0174-2.

Brun, J.P., Sokoutis, D., Van Den Driessche, J., 1994. Analogue modeling of detachment fault systems and core complexes. Geol 22, 319–322. doi:10.1130/0091-7613(1994)022<0319:AMODFS>2.3.CO;2

Buck, W.R., 1991. Modes of continental lithospheric extension. Journal of Geophysical Research: Solid Earth (1978–2012) 96, 20161–20178. doi:10.1029/91JB01485

Burg, J.-P., Ricou, L.-E., Ivano, Z., Godfriaux, I., Dimov, D., and Klain, L., 1996, Syn-metamorphic nappe complex in the Rhodope Massif. Structure and kinematics: Terra Nova, v. 8, no. 1, p. 6–15, doi: 10.1111/j.1365-3121.1996.tb00720.x.

Burov, E., Poliakov, A., 2001. Erosion and rheology controls on synrift and postrift evolution: Verifying old and new ideas using a fully coupled numerical model. J. Geophys. Res. 106, 16461–16481. doi:10.1029/2001JB000433

Boggs S Jr1995 Principles Of Sedimentology And Stratigraphy, Prentice Hall Inc., 774p

Caby, R., Hammor, D., and Delor, C., 2001, Metamorphic evolution, partial melting and Miocene exhumation of lower crust in the Edough metamorphic core complex, west Mediterranean orogen: Tectonophysics, v. 342, no. 3-4, p. 239–273, doi: 10.1016/S0040-1951(01)00166-4.

Cao, S., Neubauer, F., Bernroider, M., Liu, J., Genser, J., 2013. Structures, microfabrics and textures of the Cordilleran-type Rechnitz metamorphic core complex, Eastern Alps. Tectonophysics 608, 1201–1225. doi:10.1016/j.tecto.2013.06.025

Carmignani, L., Decandia, F.A., Disperati, L., Fantozzi, P.L., Kligfield, R., Lazzarotto, A., Liotta, D., and Meccheri, M., 2001, Inner Northern Apennines, in Anatomy of an Orogen: the Apennines and Adjacent Mediterranean Basins, Springer Netherlands, Dordrecht, p. 197–213.

Carmignani, L., Kligfield, R., 1990. Crustal extension in the northern Apennines: The transition from compression to extension in the Alpi Apuane Core Complex. Tectonics 9, 1275–1303. doi:10.1029/TC009i006p01275

Chiaraluce, L., Chiarabba, C., Collettini, C., Piccinini, D., and Cocco, M., 2007, Architecture and mechanics of an active low-angle normal fault: Alto Tiberina Fault, northern Apennines, Italy: Journal of Geophysical Research, v. 112, no. B10, p. B10310, doi: 10.1029/2007JB005015.

Chopra, P.N., Paterson, M.S., 1984. The role of water in the deformation of dunite. J. Geophys. Res. 89, 7861–7876. doi:10.1029/JB089iB09p07861

Collettini, C., Holdsworth, R.E., 2004. Fault zone weakening and character of slip along low-angle normal faults: insights from the Zuccale fault, Elba, Italy. Journal of the Geological Society 161, 1039–1051. doi:10.1144/0016-764903-179

Collettini, C., De Paola, N., Holdsworth, R.E., and Barchi, M.R., 2006, The development and behaviour of low-angle normal faults during Cenozoic asymmetric extension in the Northern Apennines, Italy: Journal of Structural Geology, v. 28, no. 2, p. 333–352, doi: 10.1016/j.jsg.2005.10.003.

Cundall, P.A., 1989. Numerische Simulation der Lokalisierung in reibungsbehaftetem Material. Ingenieur-Archiv 59, 148–159. doi:10.1007/BF00538368

Daniel, J.-M., Jolivet, L., 1995. Detachment faults and pluton emplacement; Elba Island (Tyrrhenian Sea). Bulletin de la Societe Geologique de France 166, 341–354. doi:10.2113/gssgfbull.166.4.341

Davis, G.A., Lister, G.S., Reynolds, S.J., 1986. Structural evolution of the Whipple and South mountains shear zones, southwestern United States. Geol 14, 7. doi:10.1130/0091-7613(1986)14<7:SEOTWA>2.0.CO;2

de Capitani, C., Petrakakis, K., 2010. The computation of equilibrium assemblage diagrams with Theriak/Domino software. American Mineralogist 95, 1006–1016. doi:10.2138/am.2010.3354

de Galdeano, C.S., and Vera, J.A., 1992, Stratigraphic record and palaeogeographical context of the Neogene basins in the Betic Cordillera, Spain: Basin Research, v. 4, no. 1, p. 21–35.

Denèle, Y., Lecomte, E., Jolivet, L., Lacombe, O., Labrousse, L., Huet, B., Le Pourhiet, L., 2011. Granite intrusion in a metamorphic core complex: The example of the Mykonos laccolith (Cyclades, Greece). Tectonophysics 501, 52–70. doi:10.1016/j.tecto.2011.01.013

Dèzes, P., Ziegler, P., 2001. Map of the European Moho. EUCOR URGENT.

Di Luccio, F., Pasyanos, M.E., 2007. Crustal and upper-mantle structure in the Eastern Mediterranean from the analysis of surface wave dispersion curves. Geophysical Journal International 169, 1139–1152. doi:10.1111/j.1365-246X.2007.03332.x

Dickinson, W.R., 2002. The Basin and Range Province as a Composite Extensional Domain. International Geology Review 44, 1–38. doi:10.2747/0020-6814.44.1.1

Diener, J.F.A., Powell, R., White, R.W., Holland, T.J.B., 2007. A new thermodynamic model for clino- and orthoamphiboles in the system Na2O-CaO-FeO-MgO-Al2O3-SiO2-H 2O-O. Journal of Metamorphic Geology 25, 631–656. doi:10.1111/j.1525-1314.2007.00720.x

Dilek, Y., Altunkaynak, S., Oner, Z., 2009. Syn-extensional granitoids in the Menderes core complex and the late Cenozoic extensional tectonics of the Aegean province. Geological Society, London, Special Publications 321, 197–223. doi:10.1144/SP321.10

Ferrandini, M., Ferrandini, J., Loÿe-Pilot, M.-D., Butterlin, J., Cravatte, J., and Janin, M.-C., 1998, Le Miocène du bassin de Saint-Florent(Corse): Modalités de la transgression du Burdigalien supérieur et mise en évidence du Serravallien: Geobios, v. 31, no. 1, p. 125–137, doi: 10.1016/S0016-6995(98)80102-2.

Famin, V., Philippot, P., Jolivet, L., and Agard, P., 2004, Evolution of hydrothermal regime along a crustal shear zone, Tinos Island, Greece: Tectonics, v. 23, no. 5, p. n/a–n/a, doi: 10.1029/2003TC001509.

Fournier, M., Jolivet, L., Goffé, B., and Dubois, R., 1991, Alpine Corsica Metamorphic Core Complex: Tectonics, v. 10, no. 6, p. 1173–1186, doi: 10.1029/91TC00894.

Gautier, P., Bozkurt, E., Bosse, V., Hallot, E., and Dirik, K., 2008, Coeval extensional shearing and lateral underflow during Late Cretaceous core complex development in the Niğde Massif, Central Anatolia, Turkey: Tectonics, v. 27, no. 1, p. n/a–n/a, doi: 10.1029/2006TC002089.

Gautier, P., Bozkurt, E., Hallot, E., Dirik, K., 2002. Dating the exhumation of a metamorphic dome: geological evidence for pre-Eocene unroofing of the Nigde Massif (Central Anatolia, Turkey). Geol. Mag. 139. doi:10.1017/S0016756802006751

Gautier, P., Brun, J.-P., Jolivet, L., 1993. Structure and kinematics of Upper Cenozoic extensional detachment on Naxos and Paros (Cyclades Islands, Greece). Tectonics 12, 1180–1194. doi:10.1029/93TC01131

Gerya, T.V., Yuen, D.A., 2003. Characteristics-based marker-in-cell method with conservative finite-differences schemes for modeling geological flows with strongly variable transport properties. Physics of the Earth and Planetary Interiors 140, 293–318. doi:10.1016/j.pepi.2003.09.006

Goncuoglu, M.C., Toprak, V., Kuscu, U., Erler, A., Olgun, E., 1991. Geology of the Western part of the Central Anatolian Massif, Part 1: Southern Part. Turkish Petroleum Corporation

Grasemann, B., Schneider, D.A., Stockli, D.F., Iglseder, C., 2011. Miocene bivergent crustal extension in the Aegean: Evidence from the western Cyclades (Greece). Lithosphere 4, L164.1–39. doi:10.1130/L164.1

Gueydan, F., 2003, Analysis of continental midcrustal strain localization induced by microfracturing and reaction-softening: Journal of Geophysical Research, v. 108, no. B2, p. 2064, doi: 10.1029/2001JB000611.

Gueydan, F., 2004. Mechanics of low-angle extensional shear zones at the brittle-ductile transition. J. Geophys. Res. 109, B12407. doi:10.1029/2003JB002806

Heymes, T., Bouillin, J.P., Pêcher, A., Monié, P., and Compagnoni, R., 2008, Middle Oligocene extension in the Mediterranean Calabro-Peloritan belt (southern Italy): Insights from the Aspromonte nappes pile: Tectonics, v. 27, no. 2, p. n/a–n/a, doi: 10.1029/2007TC002157.

Heymes, T., Monié, P., Arnaud, N., Pêcher, A., Bouillin, J.-P., Compagnoni, R., 2010. Alpine tectonics in the Calabrian–Peloritan belt (southern Italy): New $^{40}Ar/^{39}Ar$ data in the Aspromonte Massif area. Lithos 114, 451–472. doi:10.1016/j.lithos.2009.10.011

Hoinkes, G., Koller, F., Rantitsch, G., Dachs, E., Hock, V., Neubauer, F., Schuster, R., 1999. Alpine metamorphism of the Eastern Alps. Schweizerische Mineralogische Und Petrographische Mitteilungen 79, 155–181.

Holland, T.J.B., Powell, R., 2004. An internally consistent thermodynamic data set for phases of petrological interest. Journal of Metamorphic Geology 16, 309–343. doi:10.1111/j.1525-1314.1998.00140.x

Huang, W.L., and Wyllie, P.J., 1981, Phase relationships of S-type granite with H2O to 35 kbar: Muscovite granite from Harney Peak, South Dakota: Journal of Geophysical Research: Solid Earth (1978–2012), v. 86, no. B11, p. 10515–10529, doi: 10.1029/JB086iB11p10515.

Huet, B., Le Pourhiet, L., Labrousse, L., Burov, E., Jolivet, L., 2010. Post-orogenic extension and metamorphic core complexes in a heterogeneous crust: the role of crustal layering inherited from collision. Application to the Cyclades (Aegean domain). Geophysical Journal International 184, 611–625. doi:10.1111/j.1365-246X.2010.04849.x

Huet, B., Le Pourhiet, L., Labrousse, L., Burov, E.B., Jolivet, L., 2011. Formation of metamorphic core complex in inherited wedges: A thermomechanical modelling study. Earth and Planetary Science Letters 309, 249–257. doi:10.1016/j.epsl.2011.07.004

Isik, V., Tekeli, O., 2001. Late orogenic crustal extension in the northern Menderes massif (western Turkey): evidence for metamorphic core complex formation. Int J Earth Sci 89, 757–765. doi:10.1007/s005310000105

Isik, V., Tekeli, O., and Seyitoğlu, G., 2004, The $^{40}Ar/^{39}Ar$ age of extensional ductile deformation and granitoid intrusion in the northern Menderes core complex: implications for the initiation of extensional tectonics in western Turkey: Journal of Asian Earth Sciences, v. 23, no. 4, p. 555–566, doi: 10.1016/j.jseaes.2003.09.001.

Isık, V., Seyitoğlu, G., Çemen, İ., 2003. Ductile–brittle transition along the Alaşehir detachment fault and its structural relationship with the Simav detachment fault, Menderes massif, western Turkey. Tectonophysics 374, 1–18. doi:10.1016/S0040-1951(03)00275-0

Janák, M., Plašienka, D., Frey, M., Cosca, M., Schmidt, S.T., Lupták, B., Méres, Š., 2001. Cretaceous evolution of a metamorphic core complex, the Veporic unit, Western Carpathians (Slovakia): P–T conditions and in situ40Ar/39Ar UV laser probe dating of metapelites. Journal of Metamorphic Geology 19, 197–216. doi:10.1046/j.0263-4929.2000.00304.x

Jansen, J., 1977, The geology of Naxos.

Jaoul, O., Tullis, J., Kronenberg, A., 1984. The effect of varying water contents on the creep behavior of Heavitree quartzite. Journal of Geophysical Research: Solid Earth (1978–2012) 89, 4298–4312. doi:10.1029/JB089iB06p04298

Jolivet, L., Augier, R., Faccenna, C., Negro, F., Rimmelé, G., Agard, P., Robin, C., Rossetti, F., and Crespo-Blanc, A., 2008, Subduction, convergence and the mode of backarc extension in the Mediterranean region: Bulletin de la Societe Geologique de France, v. 179, no. 6, p. 525–550, doi: 10.2113/gssgfbull.179.6.525.

Jolivet, L., Brun, J.-P., 2008. Cenozoic geodynamic evolution of the Aegean. Int J Earth Sci 99, 109–138. doi:10.1007/s00531-008-0366-4

Jolivet, L., Dubois, R., Fournier, M., Goffé, B., Michard, A., Jourdan, C., 1990. Ductile extension in alpine Corsica. Geol 18, 1007. doi:10.1130/0091-7613(1990)018<1007:DEIAC>2.3.CO;2

Jolivet, L., Faccenna, C., Goffé, B., Burov, E., and Agard, P., 2003, Subduction tectonics and exhumation of high-pressure metamorphic rocks in the Mediterranean orogens: American Journal of Science, v. 303, no. 5, p. 353–409, doi: 10.2475/ajs.303.5.353.

Jolivet, L., Faccenna, C., Piromallo, C., 2009a. From mantle to crust: Stretching the Mediterranean. Earth and Planetary Science Letters 285, 198–209. doi:10.1016/j.epsl.2009.06.017

Jolivet, L., Goffé, B., Monié, P., and Luxey, C.T., 1996, Miocene detachment in Crete and exhumation P-T-t paths of high-pressure metamorphic rocks: Tectonics, v. 15, no. 6, p. 1129–1153.

Jolivet, L., Goffé, B., Monié, P., Luxey, C.T., 1996. Miocene detachment in Crete and exhumation P-T-t paths of high-pressure metamorphic rocks. Tectonics 15, 1129–1153.

Jolivet, L., Labrousse, L., Agard, P., Lacombe, O., Bailly, V., Lecomte, E., Mouthereau, F., Mehl, C., 2009b. Rifting and shallow-dipping detachments, clues from the Corinth Rift and the Aegean. Tectonophysics 1–18. doi:10.1016/j.tecto.2009.11.001

Jolivet, L., Lecomte, E., Huet, B., Denèle, Y., Lacombe, O., Labrousse, L., Le Pourhiet, L., Mehl, C., 2010a. The North Cycladic Detachment System. Earth and Planetary Science Letters 289, 87–104. doi:10.1016/j.epsl.2009.10.032

Jolivet, L., Trotet, F., Monié, P., Vidal, O., Goffé, B., Labrousse, L., Agard, P., Ghorbal, B., 2010b. Along-strike variations of P–T conditions in accretionary wedges and syn-orogenic extension, the HP–LT Phyllite–Quartzite Nappe in Crete and the Peloponnese. Tectonophysics 480, 133–148. doi:10.1016/j.tecto.2009.10.002

Karabulut, H., Paul, A., Ergün, T.A., Hatzfeld, D., Childs, D.M., and Aktar, M., 2013, Long-wavelength undulations of the seismic Moho beneath the strongly stretched Western Anatolia: Geophysical Journal International, v. 194, no. 1, p. 450–464, doi: 10.1093/gji/ggt100.

Kilias, A., Fassoulas, C., Mountrakis, D., 1994. Tertiary extension of continental crust and uplift of Psiloritis metamorphic core complex in the central part of the Hellenic Arc (Crete, Greece). Geol Rundsch 83, 417–430. doi:10.1007/BF00210555

Kirby, S.H., Kronenberg, A.K., 1987. Rheology of the lithosphere: Selected topics. Reviews of Geophysics 25, 1219–1244. doi:10.1029/rg025i006p01219

Koulakov, I., Sobolev, S.V., 2006. Moho depth and three-dimensional Pand Sstructure of the crust and uppermost mantle in the Eastern Mediterranean and Middle East derived from tomographic inversion of local ISC data. Geophysical Journal International 164, 218–235. doi:10.1111/j.1365-246X.2005.02791.x

Krohe, A., and Mposkos, E., 2002, Multiple generations of extensional detachments in the Rhodope Mountains (northern Greece): evidence of episodic exhumation of high-pressure rocks, in Blundell, D.J., Quadt, von, A., and Gosen, von, W. eds., Spec. Pub. Geol. Soc.p. 151–178.

Kuhlemann, J., Frisch, W., Dunkl, I., Kázmér, M., Schmiedl, G., 2004. Miocene siliciclastic deposits of Naxos Island: Geodynamic and environmental implications for the evolution of the southern Aegean Sea (Greece). Geological Society of America Special Papers 378, 51–65. doi:10.1130/0-8137-2378-7.51

Laurent, V., Beaudoin, A., Jolivet, L., Arbaret, L., Augier, R., Rabillard, A., Menant, A., 2015. Interrelations between extensional shear zones and synkinematic intrusions: The example of Ikaria Island (NE Cyclades, Greece). Tectonophysics 651-652, 152–171. doi:10.1016/j.tecto.2015.03.020

Le Maitre, R.W., 1976. The Chemical Variability of some Common Igneous Rocks. Journal of Petrology 17, 589–598. doi:10.1093/petrology/17.4.589

Le Pourhiet, L., Burov, E., Moretti, I., 2004. Rifting through a stack of inhomogeneous thrusts (the dipping pie concept). Tectonics 23, n/a–n/a. doi:10.1029/2003TC001584

Liati, A., 2005, Identification of repeated Alpine (ultra) high-pressure metamorphic events by U–Pb SHRIMP geochronology and REE geochemistry of zircon: the Rhodope zone of Northern Greece: Contributions to Mineralogy and Petrology, v. 150, no. 6, p. 608–630, doi: 10.1007/s00410-005-0038-3.

Lips, A.L.W., Cassard, D., Sebilir, H., Yilmaz, H., and Wijbrans, J.R., 2001, Multistage exhumation of the Menderes Massif, western Anatolia (Turkey): International Journal of Earth Sciences, v. 89, no. 4, p. 781–792, doi: 10.1007/s005310000101.

Lister, G.S., Davis, G.A., 1989. The origin of metamorphic core complexes and detachment faults formed during Tertiary continental extension in the northern Colorado River region, USA. Journal of Structural Geology 11, 65–94. doi:10.1016/0191-8141(89)90036-9

Lonergan, L., Platt, J.P., 1995. The Malaguide-Alpujarride boundary: a major extensional contact in the Internal Zone of the eastern Betic Cordillera, SE Spain. Journal of Structural Geology. doi:10.1016/0191-8141(95)00070-T

Marone, F., van der Meijde, M., van der Lee, S., Giardini, D., 2003. Joint inversion of local, regional and teleseismic data for crustal thickness in the Eurasia–Africa plate boundary region. Geophysical Journal International 154, 499–514. doi:10.1046/j.1365-246X.2003.01973.x

Marroni, M., Pandolfi, L., 2003. Deformation history of the ophiolite sequence from the Balagne Nappe, northern Corsica: insights in the tectonic evolution of Alpine Corsica. Geol. J. 38, 67–83. doi:10.1002/gj.933

Mattei, M., Cipollari, P., Cosentino, D., Argentieri, A., Rossetti, F., Speranza, F., and Di Bella, L., 2002, The Miocene tectono-sedimentary evolution of the southern Tyrrhenian Sea: stratigraphy, structural and palaeomagnetic data from the on-shore Amantea basin (Calabrian Arc, Italy): Basin Research, v. 14, no. 2, p. 147–168, doi: 10.1046/j.1365-2117.2002.00173.x.

Mezri, L., Le Pourhiet, L., Wolf, S., Burov, E., 2015. New parametric implementation of metamorphic reactions limited by water content, impact on exhumation along detachment faults. LITHOS 236-237, 287–298. doi:10.1016/j.lithos.2015.08.021

Michard, A., Negro, F., Saddiqi, O., 2006. Pressure–temperature–time constraints on the Maghrebide mountain building: evidence from the Rif–Betic transect (Morocco, Spain), Algerian correlations, and geodynamic implications. Comptes Rendus Geoscience 338, 92–114. doi:10.1016/j.crte.2005.11.011

Miller, E.L., Gans, P.B., Garing, J., 1983. The Snake Range Décollement: An exhumed Mid-Tertiary ductile-brittle transition. Tectonics 2, 239–263. doi:10.1029/TC002i003p00239

Moresi, L., Dufour, F., Mühlhaus, H.B., 2003. A Lagrangian integration point finite element method for large deformation modeling of viscoelastic geomaterials. Journal of Computational Physics 184, 476–497. doi:10.1016/S0021-9991(02)00031-1

Mposkos, E., 1998, Cretaceous and tertiary tectonometamorphic events in Rhodope zone (Greece): petrological and geochronological evidences: Bull Geol Soc Greece.

Okay, A.I., Satir, M., 2000. Coeval plutonism and metamorphism in a latest Oligocene metamorphic core complex in northwest Turkey. Geol. Mag. 137, 495–516.

Pamić, J., Balen, D., Herak, M., 2012. Origin and geodynamic evolution of Late Paleogene magmatic associations along the Periadriatic-Sava-Vardar magmatic belt. http://dx.doi.org/10.1080/09853111.2002.10510755 15, 209–231. doi:10.1080/09853111.2002.10510755

Pavelić, D., 2001, Tectonostratigraphic model for the North Croatian and North Bosnian sector of the Miocene Pannonian Basin System: Basin Research, v. 13, no. 3, p. 359–376, doi: 10.1046/j.0950-091x.2001.00155.x.

Piller, W.E., Harzhauser, M., and Mandic, O., 2007, Miocene Central Paratethys stratigraphy—current status and future directions: Stratigraphy, v. 13, p. 359–376.

Platt, J.P., Behrmann, J.H., Martínez, J.M.M., Vissers, R.L.M., 1984. A zone of mylonite and related ductile deformation beneath the alpujarride nappe complex, betic cordilleras, S. Spain. Geol Rundsch 73, 773–785. doi:10.1007/BF01824981

Platzman, E., and Platt, J.P., 2004, Kinematics of a twisted core complex: Oblique axis rotation in an extended terrane (Betic Cordillera, southern Spain): Tectonics,, doi: 10.1029/2003TC001549.

Plunder, A., Agard, P., Chopin, C., Okay, A.I., 2013. Geodynamics of the Tavşanlı zone, western Turkey: Insights into subduction/obduction processes. Tectonophysics 608, 884–903. doi:10.1016/j.tecto.2013.07.028

Poliakov, A.N.B., Podladchikov, Y., Talbot, C., 1993. Initiation of salt diapirs with frictional overburdens: numerical experiments. Tectonophysics 228, 199–210. doi:10.1016/0040-1951(93)90341-G

Rabillard, A., Arbaret, L., Jolivet, L., Le Breton, N., Gumiaux, C., Augier, R., Grasemann, B., 2015. Interactions between plutonism and detachments during metamorphic core complex formation, Serifos Island (Cyclades, Greece). Tectonics 34, 1080–1106. doi:10.1002/2014TC003650

Ranalli, G., Murphy, D.C., 1987. Rheological stratification of the lithosphere. Tectonophysics 132, 281–295. doi:10.1016/0040-1951(87)90348-9

Ratschbacher, L., Frisch, W., Linzer, H.G., and Merle, O., 1991, Lateral extrusion in the eastern Alps, PArt 2: Structural analysis: Tectonics, v. 10, no. 2, p. 257–271, doi: 10.1029/90TC02623.

Rey, P.F., Teyssier, C., Kruckenberg, S.C., Whitney, D.L., 2011. Viscous collision in channel explains double domes in metamorphic core complexes. Geol 39, 387–390. doi:10.1130/G31587.1

Rey, P.F., Teyssier, C., Whitney, D.L., 2009. Extension rates, crustal melting, and core complex dynamics. Geol 37, 391–394. doi:10.1130/G25460A.1

Ring, U., Johnson, C., Hetzel, R., and Gessner, K., 2003, Tectonic denudation of a Late CretaceousTertiary collisional belt: regionally symmetric cooling patterns and their relation to extensional faults in the Anatolide belt of western Turkey: Geological Magazine, v. 140, no. 4, p. 421–441, doi: 10.1017/S0016756803007878.

Rohais, S., Eschard, R., Ford, M., Guillocheau, F., and Moretti, I., 2007, Stratigraphic architecture of the Plio-Pleistocene infill of the Corinth Rift: Implications for its structural evolution: Tectonophysics, v. 440, no. 1-4, p. 5–28, doi: 10.1016/j.tecto.2006.11.006.

Rossetti, F., Goffé, B., Monié, P., Faccenna, C., Vignaroli, G., 2004. Alpine orogenic P-T-t-deformation history of the Catena Costiera area and surrounding regions (Calabrian Arc, southern Italy): The nappe edifice of north Calabria revised with insights on the Tyrrhenian-Apennine system formation. Tectonics 23, n/a–n/a. doi:10.1029/2003tc001560

Royden, L.H., 1993, Evolution of retreating subduction boundaries formed during continental collision: Tectonics, v. 12, no. 3, p. 629–638, doi: 10.1029/92TC02641.

Saadallah, A., Caby, R., 1996. Alpine extensional detachment tectonics in the Grande Kabylie metamorphic core complex of the Maghrebides (northern Algeria). Tectonophysics 267, 257–273. doi:10.1016/S0040-1951(96)00101-1

Sanchez-Gomez, M., Avigad, D., and Heimann, A., 2002, Geochronology of clasts in allochthonous Miocene sedimentary sequences on Mykonos and Paros Islands: implications for back-arc extension in the Aegean Sea: Journal of the Geological Society, v. 159, no. 1, p. 45–60, doi: 10.1144/0016-764901031.

Schenker, F.L., Gerya, T., and Burg, J.P., 2012, Bimodal behavior of extended continental lithosphere: Modeling insight and application to thermal history of migmatitic core complexes: Tectonophysics, v. 579, no. C, p. 88–103, doi: 10.1016/j.tecto.2012.07.002.

Sorel, D., 2000, A Pleistocene and still-active detachment fault and the origin of the Corinth–Patras rift, Greece: Geology, v. 28, p. 83–86.

Souche, A., Medvedev, S., Andersen, T.B., and Dabrowski, M., 2013, Shear heating in extensional detachments: Implications for the thermal history of the Devonian basins of W Norway: Tectonophysics, v. 608, p. 1073–1085, doi: 10.1016/j.tecto.2013.07.005.

Soukis, K., and Stockli, D.F., 2013, Structural and thermochronometric evidence for multi-stage exhumation of southern Syros, Cycladic islands, Greece: Tectonophysics, v. 595-596, p. 148–164, doi: 10.1016/j.tecto.2012.05.017.

Sümer, Ö., İnci, U., and Sözbilir, H., 2013, Tectonic evolution of the Söke Basin: Extension-dominated transtensional basin formation in western part of the Büyük Menderes Graben, Western Anatolia, Turkey: Journal of Geodynamics,, doi: 10.3166/ga.19.363-390.

Tan, E., Lavier, L.L., Van Avendonk, H.J.A., Heuret, A., 2012. The role of frictional strength on plate coupling at the subduction interface. Geochem. Geophys. Geosyst. 13, n/a–n/a. doi:10.1029/2012GC004214

Tiberi, C., Diament, M., Lyon-Caen, H., King, T., 2001. Moho topography beneath the Corinth Rift area (Greece) from inversion of gravity data. Geophysical Journal International 145, 797–808. doi:10.1046/j.1365-246x.2001.01441.x

Tirel, C., Brun, J.-P., Burov, E., 2008. Dynamics and structural development of metamorphic core complexes. J. Geophys. Res. 113, B04403. doi:10.1029/2005JB003694

Tirel, C., Brun, J.P., Sokoutis, D., 2006. Extension of thickened and hot lithospheres: Inferences from laboratory modeling. Tectonics 25, n/a–n/a. doi:10.1029/2005TC001804

Trotet, F., Jolivet, L., Vidal, O., 2001. Tectono-metamorphic evolution of Syros and Sifnos islands (Cyclades, Greece). Tectonophysics 338, 179–206. doi:10.1016/S0040-1951(01)00138-X

Ustaszewski, K., Kounov, A., Schmid, S.M., Schaltegger, U., Krenn, E., Frank, W., Fügenschuh, B., 2010. Evolution of the Adria-Europe plate boundary in the northern Dinarides: From continent-continent collision to back-arc extension. Tectonics 29,. doi:10.1029/2010TC002668 van Hinsbergen, D.J.J., 2010. A key extensional metamorphic complex reviewed and restored: The Menderes Massif of western Turkey. Earth-Science Reviews 102, 60–76. doi:10.1016/j.earscirev.2010.05.005

Vanderhaeghe, O., 2004. Structural development of the Naxos migmatite dome. Geological Society of America Special Papers 380, 211–227. doi:10.1130/0-8137-2380-9.211

Whitney, D.L., Dilek, Y., 1997. Core complex development in central Anatolia, Turkey. Geol 25, 1023. doi:10.1130/0091-7613(1997)025<1023:CCDICA>2.3.CO;2

Whitney, D.L., Teyssier, C., Rey, P., and Buck, W.R., 2013, Continental and oceanic core complexes: Geological Society of America Bulletin, v. 125, no. 3-4, p. 273–298, doi: 10.1130/B30754.1.

Wu, G., Lavier, L.L., Choi, E., 2015. Modes of continental extension in a crustal wedge. Earth and Planetary Science Letters 421, 89–97. doi:10.1016/j.epsl.2015.04.005

Yamato, P., Agard, P., Burov, E., Le Pourhiet, L., Jolivet, L., Tiberi, C., 2007. Burial and exhumation in a subduction wedge: Mutual constraints from thermomechanical modeling and natural P-T-t data (Schistes Lustrés, western Alps). J. Geophys. Res. 112, B07410. doi:10.1029/2006JB004441

1. Locality		**A- Betics**, Spain		**B- Beni Bousera** (B.B.), Morocco
2. Upper plate	2.1 Syntectonic basin		continental to marine (de Galdeano and Vera, 1992)	
	2.2 Basal lithologies	**Malaguides** : palaeozoic sandstones and slates	**Alpujarrides** : phyllites, quartzites and graphitic micaschists	**Ghomarides** : paleozoic metasediments
	2.3 Peak metamorphic conditions	lower anchizone (variscan)	HPA in Herradura to GS in Lujar Gador (Azañón and Crespo-Blanc, 2000; Jolivet et al., 2010b)	GS ?
	2.4 Brittle deformation		2 sets of LANF (Platzman and Platt, 2004; Augier et al., 2005)	
3. Detachment Zone	3.1 Abbreviation/name	MAD/**Malaguides-Alpujarrides Detachment** (Platzman and Platt, 2004)	MFSZ/**Mecina-Filabres Shear Zone** (Platt et al., 1984)	ZaFZ/**Zaouia Fault Zone**
	3.2 Associated lithologies	Calc-mylonites and fault gauge (Lonergan and Platt, 1995)	mylonites and gouges	« brittle-ductile fault » (Michard et al., 2006)
	3.3 Relationships to heritage	reactivated thrust	reactivated thrust	oblique to thrusts
4. Lower plate	4.1 Top lithologies	**Alpujarrides** : phyllites, quartzites and graphitic micaschists	**Nevado-Filabrides** : permo-triassic graphitic schists (Bedar Macael)	**Sebtides** : permo-triassic metasediments (Filali schists & Federico)
	4.2 Peak metamorphic conditions*	HPA in Herradura (Alpu1) to GS in Lujar Gador (Alpu4) (Azañón and Crespo-Blanc, 2000)	E in Bedar Macael (NF1) to GS in Ragua (NF3, Augier et al., 2005)	HPA in Federico (BB3) HPG in B.B. kinzigites (BB2)
	4.3 Brittle deformation			
5. Migmatites		at the base of Herradura	no HT overprint	
6. Intrusives	6.1 Type	mafic dikes in upper and lower plates		leucogranite dikes in B.B. lower u.
	6.2 Relation to ductile deformation	late ? magmatism		undeformed
7. Ophiolitic units	7.1 Type			peridotites
	7.2 Position			in the dome core
8. Timing in orogeny		syn-orogenic initiation (Jolivet et al., 2008)	mainly post-orogenic (Jolivet et al., 2008)	possibly syn-orogenic (Michard et al., 2006)
9. Geodynamic boundary conditions		change of slab retreat direction from southward to westward		Alboran slab retreat

Table 1a

1.		**C- Grande Kabylie**, Algeria	**D- Edough,** Algeria	**E- Aspromonte,** S. Italy	**F- Catena Costiera**, S. Italy
2.	2.1	Kabylian oligo-miocene marine conglomerates (OMK)	none	continental to marine Stilo-Capo d'Orlando Formation (SCOF) (Bonardi et al., 1980)	Miocene to Q. marine b. (e. g. Amantea b. (Mattei et al., 2002)
	2.2	pre-permian phyllites	Tellian and Green Schist facies Unit GFU (Caby et al., 2001)	**Stilo u.** : para- and orthogneiss	Upper Ophiolitic U. (UOU) : ophiolitic melange & Verbicaro carbonates (Bonardi et al., 2001)
	2.3	variscan GS	GS	vasriscan GS to A, no Alpine overprint (Heymes et al., 2008)	GS
	2.4	normal faults in Central and Eastern Grande Kabylie			tilted blocks at the base of basin
3.	3.1	KaD/**Kabylian Detachment** (Saadallah and Caby, 1996)	Ed/~KaD, major metamorphic gap	Asp/	CatCo/
	3.2	mylonites and younger cataclaistes	GS mylonites, fibrolites bearing ultra-mylonites at base of APU	mylonitic gneiss	mylonites and cataclasites (Rossetti et al., 2004)
	3.3		reactivated Tellian thrust	reactivated thrust	
4.	4.1	**Sidi Ali Boud Nab** massif: Micaschists and orthogneiss	high grade metasedimentary U. (HGMU) Amphibolite-Peridotite U. (APU) Migmatite-Granite U. (MGU)	**Aspromonte u.** : para and orthogneiss	Continental metaclastics and marbles Lower Ophiolitic U. (LOU)
	4.2	A (GK1 & GK2)	HPG	Alpine BS over variscan LPA	BS (Rossetti et al., 2004)
	4.3				
5.		anatectic metapelites	syn-tectonic anatexis in MGU	none	none
6.	6.1	aplo-pegmatites and leucogranites	leucogranites	none	none
	6.2	syn-kinematic aplites / late granites	syn-kinematic in MGU		
7.	7.1		peridotites at the base of APU (Bosch et al., 2014)	none	ophiolitic melanges, pillow-lavas and picrites in Verbicaro
	7.2		top lower plate and lenses in core		in lower and upper plates
8.		post-orogenic	late post-orogenic	syn-to immediate post-o. (Heymes et al., 2010)	post-orogenic (Jolivet et al., 2008)
9.		Alboran slab retreat	Alboran slab retreat or later slab dynamics (Bruguier, 2009)	stretching oblique to inferred slab retreat direction	E-W stretching parallel to local slab retreat in miocene

Table 1b

1.		**G- Alpi Apuane**, N. Italy	**H- Elba**, Thyrrenian sea	**I- Corsica**, W. Mediterranean	
2.	2.1	marine « Brecce delle Versilia » (Carmignani and Kligfield, 1990)	-	-	St Florent b. continental to marine limestones (Ferrandini et al., 1998)
	2.2	**Tuscan nappes** : carbonates with flysch on top	Upper Toscan ophiolite and flysch u.	**Balagne-Nebbio unit** : ophiolitic unit	**Schistes Lustrés (SL)** : calcschists, ophiolitic and continental basement slices
	2.3	no alpine metamorphism	weak thermometamorphism	non metamorphic	BS to E
	2.4	H & LANF rooting on detachment	**Zuccale Fault** : LANF with cataclasites & calcmylonites crosscuts CaDZ (Collettini and Holdsworth, 2004)	late normal faults (D5, Marroni and Pandolfi, 2003)	
3.	3.1	CalCa/**Calcare Cavernoso** (Carmignani and Kligfield, 1990)	CaDZ/**Capanne Detachment Zone** (Daniel and Jolivet, 1995)	Bal/	TeSZ/**Tenda Upper Shear Zone** (Jolivet et al., 1990; Gueydan, 2003; Fournier et al., 1991)
	3.2	mylonites & cataclasites from anhydrite and dolostone	mylonites within thermometamorphic aureole		mylonites
	3.3	reactivated thrust	oblique to thrusts	reactivated basal thrust (D4, Marroni and Pandolfi, 2003)	reactivated basal thrust
4.	4.1	**Massa** & « **Autochthonous** » **u.** : paleozoic phyllites and metasandstones	**Lower Tuscan u.** : Calamite paleozoic schists	**Schistes Lustrés (SL)** : calcschists, ophiolitic and continental basement slices	Tenda massif : palaeozoic granitoid
	4.2	BS (AA1 and AA2)	GS and thermometamorphism	BS to E	BS (Te)
	4.3				
5.		none	none	none	none
6.	6.1	volcanism 7 Ma younger (Carmignani et al., 2001)	granodiorite (Monte Capanne)	Sisco lamproïtes in SL	
	6.2			18 Ma younger than extension (Beccaluva et al., 2004)	
7.	7.1	Liguride ophiolites		Nebbio and SL ophiolites	
	7.2	top of upper plate, limited extensional reactivation		uppermost (Balagne)	
8.		post-orogenic		post-orogenic	
9.		Thyrrenian slab retreat		Thyrrenian slab retreat	

Table 1c

1.		**J- Motajica** window, Bosnia and Hercegovina	**K- Rechnitz window** area, Austria/Hungary	**L- Central Western Carpathians**, Slovakia	**M- Southern Rhodope,** Greece
2.	2.1	Ottnangian syn-rifts sediments : alluvial to marine } (Pavelić, 2001)	Fürstenfeld (W) and Danube (E) basins : transitional Karpatian deposits (Piller et al., 2007)		
	2.2	**Sava Zone** metasediments and ophiolites at the base of Tisza-Dacia u. (Ustaszewski et al., 2010)	**Wechsel u.** (base of Autro-Alpine) gneiss and Palaeozoic carbonates (Cao et al., 2013)	**Gemeric u.** : palaeozoic basement rocks	**Vertiskos Gneiss Complex** : gneiss **+ Therma and Volvi gabbros**
	2.3	A to GS	GS	low grade	(U)HP (Liati, 2005)
	2.4	late brittle normal faults	HANF		upper Miocene faulting
3.	3.1	MoD/**Motajica Detachment** (Ustaszewski et al., 2010)	ReW/	LuL/**Lubenik Line** (Janák et al., 2001)	KerD/**Kerdylion Detachment** (Brun and Sokoutis, 2007)
	3.2	Upper GS foliation in paragneiss	Serpentinite and quartz-micas mylonites (Cao et al., 2013)	mylonites from cover u. and topmost intrusive granitoid	mylonites and ultra-mylonites
	3.3	Partly reactivated thrust	possibly reactivated basal AA thrust	reactivated thrust	
4.	4.1	Accretionary wedge complex and Motajica granite	**Rechnitz ophiolite u.** Penninic greenschist and serpentinites.	**Veporic u.** : pre-Alpine basement and phyllite cover	**Southern Rhodope Core Complex :** marbles and orthogneiss
	4.2	A 5mot) and local contact metamorphism	BS (Re1) and subsequent GS (Re2)	A (Ve) and contact metamorphism	A (Barrovian gradient SRho)
	4.3		Chlorite breccias in borehole		upper Miocene faulting
5.		none	none	hercynian remnants	in the Kerdylion massif
6.	6.1	S- to I-type Motajica granite (Pamić et al., 2012)	none	Rochovce granite	Vrondou and Symvolon granodiorites
	6.2	crystallization 5 Myrs prior to extension onset		syn-tectonic	syn-kinematic
7.	7.1	Western Vardar ophiolite complex	Serpentinite, metagabbro, ophicarbonates	none	Volvi and Therma metabasites : gabbros and basalts
	7.2	Upper level of upper plate	within lower plate		base of the upper plate
8.		post-orogenic Pannonian extension	post-orogenic Pannonian extension ?	Cretaceous syn-orogenic	post-orogenic
9.		Carpathian subduction roll-back (Royden, 1993)	Eastward lateral extrusion (Ratschbacher et al., 1991) and Carpathian roll-back	Growth of collision wedge after Meliata suture	

Table1d

1.		**N- Eastern Rhodope,** Greece	**O- Northern Cyclades,** Greece (Andros-Tinos-Mikonos-Ikaria)	**P- Syros,** Greece	**Q- Central Cyclades,** Greece (Naxos Paros)
2.	2.1	**Krumovgrad** grp : colluvial to marine (Bonev et al., 2006)	marine molasses then conglomerates on Mykonos (Sanchez-Gomez et al., 2002)		from marine sanstones and pelites toward fluvial deposits (Kuhlemann et al., 2004; Bargnesi et al., 2013)
	2.2	**Kimi Complex** : high grade rocks + meta-ophiloitic lenses.	**Upper Cycladic Nappe**: ophiolitic complex (UCN)	**Vari unit and "Upper Unit"** metabasites, gneiss and serpentinites (Soukis and Stockli, 2013)	ophiolite nappe and neritic limestones
	2.3	(U?)HP 73 Ma (Krohe and Mposkos, 2002)	GS	HT (Jolivet and Brun, 2008)	unmetamorphosed
	2.4	HANF offsetting detachment	HANF branching on detachment	late brittle LANF	synthetic normal faults
3.	3.1	ToKeD/**Tokachka and Kechros detachments**	NCDS/**North Cycladic Detachment System** (Jolivet et al., 2010a)	VaD/**Vari Detachment**	NaPaD/**Naxos Paros Detachment** (Gautier et al., 1993)
	3.2	mylontes	mylonites, cataclasites and breccias	mylonites and late breccias	mylonites and ultra-mylonites
	3.3		partly reactivating UCN thrust		reactivated thrust
4.	4.1	**Kesebir-Kardamos** and **Kechros** complexes: migmatitic gneiss and orthogneiss (Bonev et al., 2006)	**Cycladic Blusechist Unit:** metapelites and marbles on granitic basement	Cycladic Blueschist Unit : metapelites, marbles metaflysch (Bonneau, 1984)	Pre-Alpine Gneiss basement with marbles and schists.
	4.2	lower E (ERho1,Mposkos, 1998)	E-BS (Tin1 to 3) then A (Mykonos and Ikaria; Ik)	E (Syr1)-BS (Syr2) (Trotet et al., 2001)	E then A (Nax 1&2, Avigad, 1998)
	4.3	HANF offsetting detachment			
5.		in Kardamos complex	on Dilos, Mykonos and Ikaria	none	pervasive melting (Vanderhaeghe, 2004)
6.	6.1	Papikion granitoid	I-type granites on Tinos, Mykonos and Ikaria (JOLIVET)	none	granodiorite (Naxos) and leucogranites (Paros)
	6.2	presumably syn-tectonic	syn- to late-tectonic		syn-extensional leucogranite
7.	7.1	Metaophiolite lenses	serpentinites, gabbros and basalts	metabasites of the Upper Unit	gabbros and ultramafics (Jansen, 1977)
	7.2	at the base of upper plate (Burg et al., 1996)	at the base of the upper plate	below early then above late detachment (Soukis and Stockli, 2013)	at the base of the upper plate
8.		syn-orogenic	post-orogenic	mainly syn-orogenic	post-orogenic
9.		Vardar ocean closure	Aegean back-arc extension		Aegean back-arc extension

Table1e

1.		**R- SouthWestern Cyclades,** Greece (Kea-Kythnos-Serifos)	**S- Kazdag**, Turkey	**T- Menderes**, Turkey	
2.	2.1	possibly on Milos	**Küçükkuyu Fm** : fluvio-lacustrine to turbidites (Bonev and Beccaletto, 2007)	Late deposits only	lacustrine to shallow marine supra-detachment basins (Sümer et al., 2013)
	2.2	**Pelagonian unit** : serpentinite and schists	**Cetmi melange** : opiolitic melange (Beccaletto and Steiner, 2005)	Ismir-Ankara Ophiolite, HP-LT nappes at the base	Northern and Southern Menderes
	2.3	A-GS	E blocks in the melange	E-BS in Afyon, Tavsanli and Oren nappes (Plunder et al., 2013)	A
	2.4	HANF	HANF crosscutting detachment	HANF bounding Simav graben	Half-grabens on both sides
3.	3.1	WCDS/**Western Cycladic Detachment System** (Grasemann et al., 2011)	AlSeD/**Alakeçi** SZ (N) and **Selale Detachment** (S)	SiD/**Simav Detachment** (Isik and Tekeli, 2001)	AlBuD/**Alasehir & Buyuk Detachments**
	3.2	(ultra)mylonites from marbles and schists	mylonites, metaserpentinites and breccias	mylonites	rmylonites only along Alasehir (Isık et al., 2003) abundant cataclasites
	3.3	reactivated thrusts ?	thrust ?	reactivated thrusts	cut through Menderes units
4.	4.1	**Cycladic Blueschist Unit**	High grade basement	**Northern Menderes**: Selimiye metasedimentary unit on top	Central Menderes
	4.2	BS then GS	A (Kaz, Okay & Satir, 2000)	A (Me4)	A
	4.3	HANF			
5.		none	at the top of the dome	inherited in the core (Schuiling, 1962)	?
6.	6.1	I-type granodiorite (Serifos and Lavrion)	Evciler calc-alcaline granite	Early northern MEG	Later central MEG
	6.2	syn- to late tectonic	intrudes ASZ	syntectonic to SiD (Isik et al., 2004)	syn-extensional (Dilek et al., 2009)
7.	7.1	serpentinites	Cetmi, Karakaya, and Denizgôren	Ismir-Ankara Ophiolite	none
	7.2	within the upper plate	at the base of the upper plate	Within the upper plate	
8.		post-orogenic	post-orogenic	post-orogenic	later post-orogenic
9.		Aegean back-arc extension	Anatolian back-arc extension	Eastern termination of NCDS (JOLIVET)	Intra-Menderes stretching (van Hinsbergen, 2010)

Table1f

1.		**U- Corinth Rift**, Greece	**V- Crete**, Greece	**W- Nigde**, Turkey
2.	2.1	fluvio-lacustrine toward marine (Rohais et al., 2007)	possibly lacustrine breccias at the base of Neogene basins (Jolivet et al., 1996)	shallow marine deposits in the late Ulukisla basin (Gautier et al., 2008)
	2.2	**Gavrovo-Tripolitza (GT)** carbonates with **Tyros beds (TB)** shales at the base	**Gavrovo-Tripolitza** carbonates	Massive ophiolite, mostly gabbros (Goncuoglu et al., 1991)
	2.3	GS (Jolivet et al., 2010b)	unmetamorphosed	GS at the base
	2.4	Zaroukla cataclastic devollement between GT and TB (Sorel, 2000)	HANF cutting across DZ	
3.	3.1	CrD1/**Cretan Detachment** (Jolivet et al., 2009)	CrD2/ (Kilias et al., 1994)	NiD
	3.2	high strain phyllites	mylonites from the upper plate	mylonites to ultracataclasites
	3.3	reactivated thrust	reactivated thrust	recativated obduction thrust
4.	4.1	**Phyllites-Quartzites**	**Phyllites-Quartzites** nappe on top of Plattenkalk	**Gumusler Formation** : migmatites
	4.2	BS	BS	A (Nig, Whitney and Dilek, 1997)
	4.3	Rift faults cutting across detachment		
5.		none	none	most of the lower plate
6.	6.1	none	none	Uçkapili leucogranite
	6.2			mainly post-tectonic (Gautier et al., 2002)
7.	7.1	none	ophiolite Asterousia nappe	massive ophiolite in the upper plate,
	7.2		on top of upper plate	dilascerated slivers in the lower plate
8.		syn- to post-orogenic	syn-orogenic (Jolivet et al., 1996)	syn-orogenic ?
9.		early Aegean extension	Aegean back-arc extension	Central Anatolian edge extension

Table1g

Locality	A		B	C	D	E	F	G	H	I		J	K	L	MN		O	P	Q	R	S	T		U	V	W
Detachment	MAD	MFSZ	ZaFZ	KaD	Ed	Asp	CatCo	CalCa	CaDZ	Bal	TeSZ	MoD	ReW	LL	KnD	ToKeD	NCDS	VD	NPD	WCDS	AlSeD	SiD	AlBuD	CrD1	CrD2	NiD
Mylonites	c	✔	✔	✔	✔	✔	c	c	✔	?	✔	✔	✔	✔	✔	✔	✔	?	✔	✔	✔	✔	?		✔	✔
1-Migmatites				✔	✔										✔	✔			✔		✔	✔				✔
2-HT lower plate			✔	✔	✔							✔		✔	✔	✔			✔		✔	✔	✔			✔
3-synD intrusives									✔			✔			✔	✔	✔		✔			✔	✔			✔
4-HP-LT in the l. plate	✔	✔				✔	✔	✔		✔	✔		✔				✔	✔	✔	✔		✔		✔	✔	
5-Resistive u. plate								✔		✔	✔	✔				✔					✔	✔				✔
syn or post-orogenic initiation	S	P	S	P	P	P	P	P	P	P	P	S		S	P	S	P	S	P	P	P	P	P	P	S	S

		Crust		Mantle
density at 25°C ($kg.m^{-3}$)		2700		3300
thermal conductivity ($W.m^{-1}.K^{-1}$)		2.5		3.3
Thermal expansion coefficient (K^{-1})			3.0×10^{-5}	
Specific heat ($J.kg^{-1}.K^{-1}$)			10^{3}	
Shear modulus (GPa)			30	
Poisson's ratio			0.25	
Mohr-Coulomb criterion			20	
Cohesion (MPa)			20	
Friction angle (°)			30	
A ($MPa^{-n}.s^{-1}$)	$1.26\ 10^{-3}$	$6.7\ 10^{-7}$	$2.51\ 10^{-4}$	2.5×10^{4}
n	2.4	2.4	2.3	3.5
E ($kJ.mol^{-1}$)	219	156	154	532
Lithology	quartz-diorite	quartzite	wet quartzite	dunite

table 3

Model	Ductile-brittle transition depth	Initial Moho temperature	Intra-crustal Strength Contrast	Integrated Lithospheric Strength	Extension Mode
units	[km]	[°C]		[MPa x km]	
Homogeneous crust :					
upper/lower crust _thickness [km]_Tbottom [° C]			d: quartz-diorite, q: quartzite, w: wet quartzite		
d/d_30_1000	26.4	398	4	33739	R
d/d_30_1200	22.3	477	17	20860	R
d/d_30_1400	19.4	557	61	12846	R
d/d_45_1000	27.5	569	103	23239	X
d/d_45_1200	23.3	683	413	9688	WR
d/d_45_1400	20.3	797	1232	5437	WR
d/d_60_1000	28.7	725	822	11564	WR
d/d_60_1200	24.3	870	2832	7244	DDC
d/d_60_1400	21.1	1015	7304	5426	DDC
q/q_30_1000	18.4	398	31	30412	R
q/q_30_1200	15.7	477	93	18245	R
q/q_30_1400	13.7	557	223	10834	R
q/q_45_1000	19.2	569	350	19165	WR
q/q_45_1200	**16.4**	**683**	**914**	**6761**	**WR**
q/q_45_1400	14.3	797	1924	3227	WR
q/q_60_1000	20.0	725	1559	7119	DDC
q/q_60_1200	17.0	870	3618	4062	DDC
q/q_60_1400	14.9	1015	6918	3026	DDC
w/w_30_1000	15.3	398	135	29119	R
w/w_30_1200	13.0	477	414	17274	WR
w/w_30_1400	11.4	557	1029	10079	WR
w/w_45_1000	16.0	569	1616	17720	WR
w/w_45_1200	13.6	683	4348	5697	DDC
w/w_45_1400	11.9	797	9443	2405	DDC
w/w_60_1000	16.6	725	7478	5554	DDC
w/w_60_1200	14.1	870	17909	2912	DDC
w/w_60_1400	12.3	1015	15913	2138	DDC
Even layered crust					
d/q_30_1000	18.4	398	31	30412	R
d/q_30_1200	15.7	477	93	18245	R
d/q_30_1400	**15.1**	**557**	**244**	**10950**	**R**
d/q_45_1000	22.6	569	409	19757	WR
d/q_45_1200	**22.5**	**683**	**1229**	**8313**	**PDC**
d/q_45_1400	20.3	797	2664	5123	PDC
d/q_60_1000	28.7	725	2195	10504	DDC
d/q_60_1200	24.3	870	5060	7066	DDC
d/q_60_1400	21.1	1015	9564	5385	DDC
d/w_30_1000	15.3	398	135	29119	X
d/w_30_1200	15.1	477	475	17506	R

d/w_30_1400	15.1	557	1329	10688	R
d/w_45_1000	22.6	569	2232	19419	X
d/w_45_1200	**22.5**	**683**	**6943**	**8217**	**DDC**
d/w_45_1400	20.3	797	15448	5089	DDC
d/w_60_1000	28.7	725	12530	10419	DDC
d/w_60_1200	24.3	870	29764	7041	DDC
d/w_60_1400	21.1	1015	26204	5375	DDC

Uneven layered crust :
upper crust/lower crust_upper thickness/total thickness [km]_Tbottom [°C]

d/q_15/45_1000	19.2	569	350	19165	WR
d/q_15/45_1200	16.4	683	914	6761	WR
d/q_15/45_1400	15.1	797	2023	3268	DDC
d/q_30/45_1000	27.5	569	492	22579	R
d/q_30/45_1200	23.3	683	1270	9576	PDC
d/q_30/45_1400	20.3	797	2664	5411	PDC

table 4

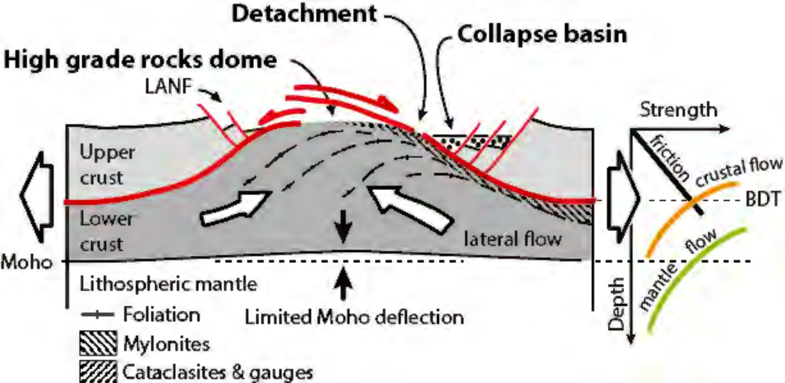
Detachment
Collapse basin
High grade rocks dome
LANF
Upper
crust
Lower
crust
Moho
Lithospheric mantle
lateral flow
Limited Moho deflection
Strength
friction
crustal flow
BDT
mantle flow
Depth
Foliation
Mylonites
Cataclasites & gauges

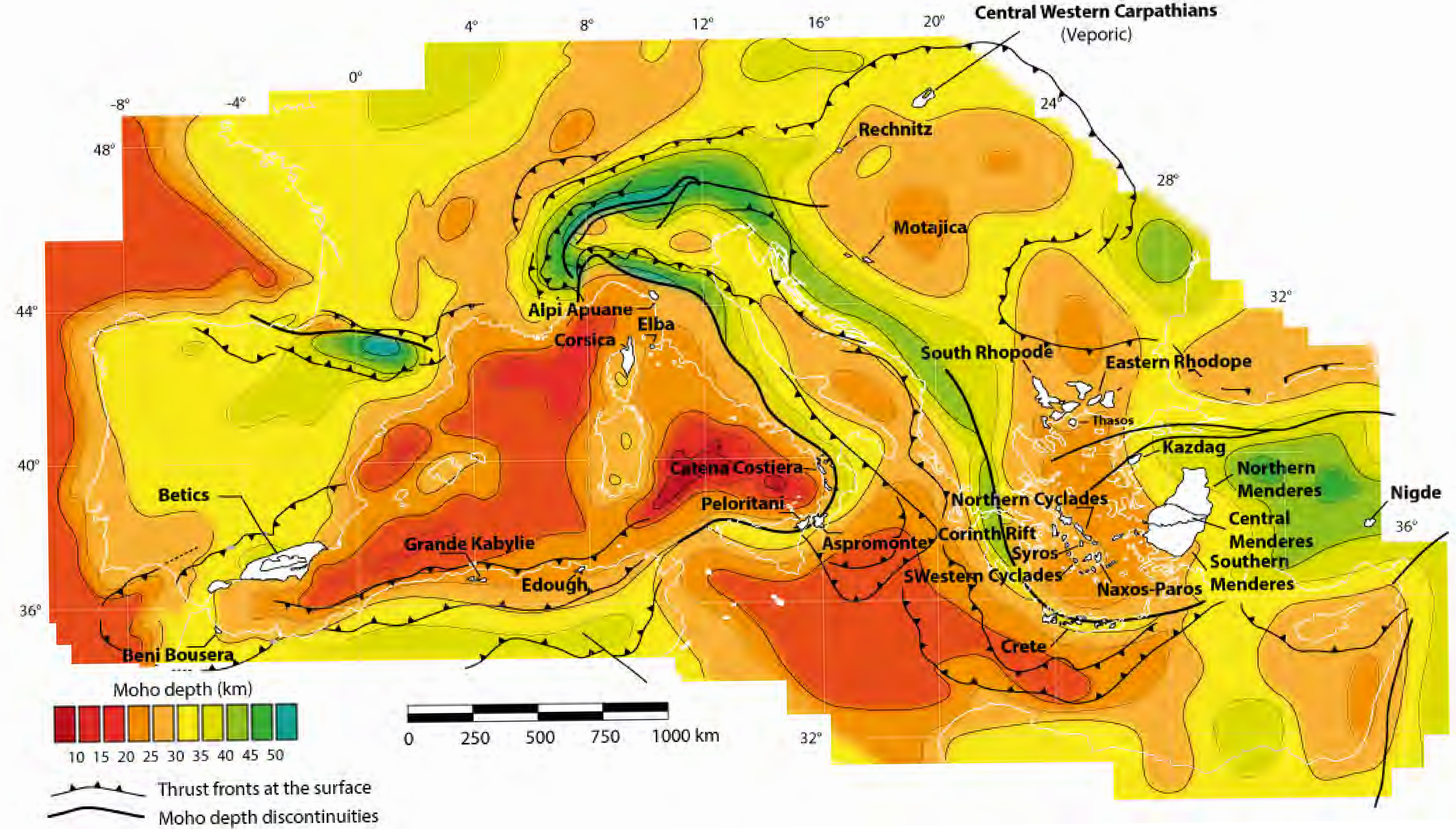
Central Western Carpathians
(Veporic)
Rechnitz
Motajica
Alpi Apuane
Elba
Corsica
South Rhopode
Eastern Rhodope
Thasos
Kazdag
Northern
Menderes
Nigde
Central
Menderes
Southern
Menderes
Betics
Catena Costiera
Peloritani
Northern Cyclades
Corinth Rift
Syros
Aspromonte
Grande Kabylie
Edough
SWestern Cyclades
Naxos-Paros
Crete
Beni Bousera
Moho depth (km)
10 15 20 25 30 35 40 45 50
0 250 500 750 1000 km
Thrust fronts at the surface
Moho depth discontinuities
-8°
-4°
0°
4°
8°
12°
16°
20°
24°
28°
32°
48°
44°
40°
36°

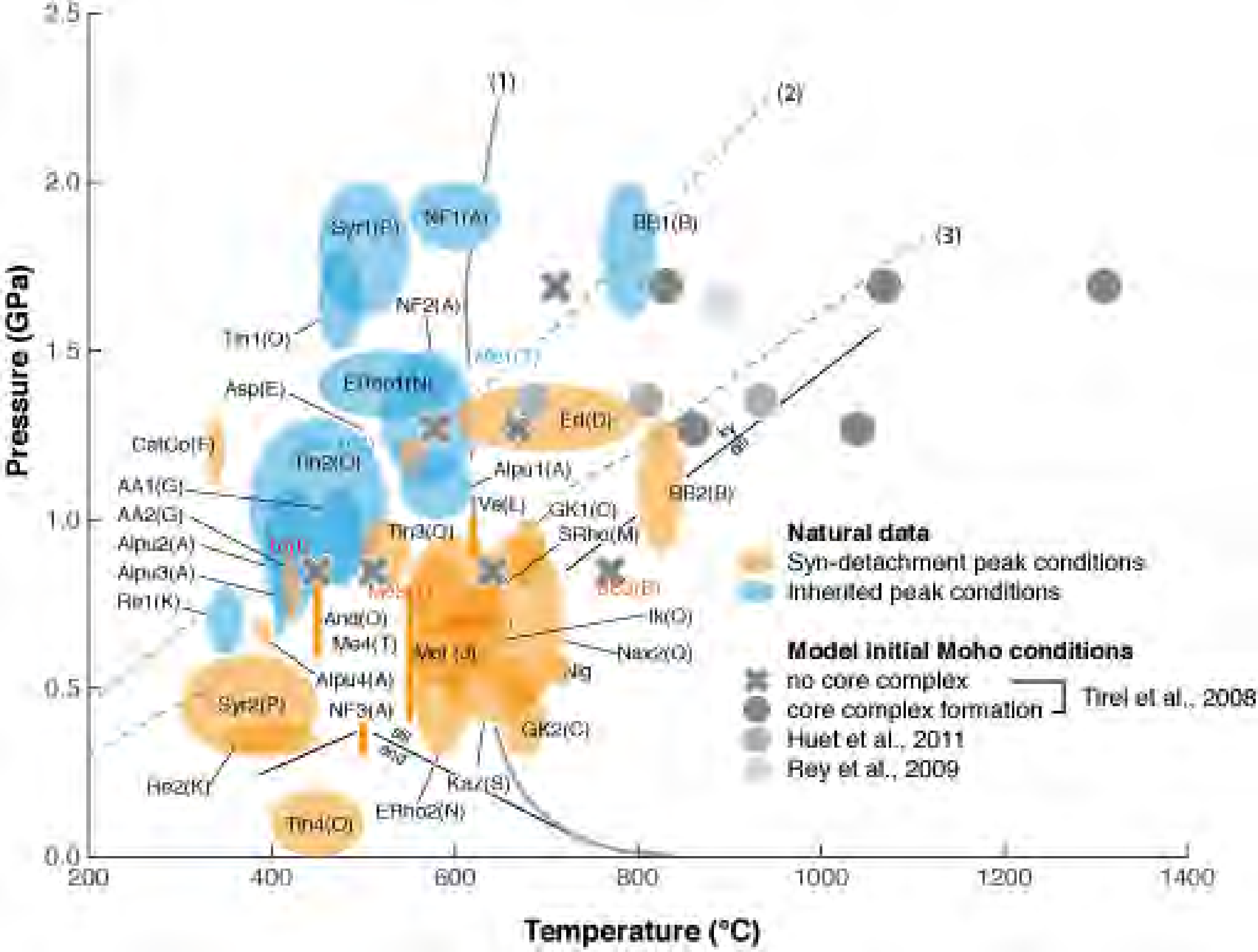

Pressure (GPa)
Temperature (°C)
0.0
0.5
1.0
1.5
2.0
2.5
200
400
600
800
1000
1200
1400
(1)
(2)
(3)
Syr1(P)
NF1(A)
BB1(B)
NF2(A)
Tin1(O)
ERho1(N)
Asp(E)
Erl(D)
CalCo(F)
Tin2(O)
Alpu1(A)
AA1(G)
Ve(L)
GK1(C)
BB2(B)
AA2(G)
Tin3(O)
SRho(M)
Alpu2(A)
Alpu3(A)
Re1(K)
And(O)
Me4(T)
Ik(O)
Naz2(O)
Alpu4(A)
Ng
Syr2(P)
NF3(A)
GK2(C)
Re2(K)
Raz(S)
ERho2(N)
Tin4(O)
Natural data
Syn-detachment peak conditions
Inherited peak conditions
Model initial Moho conditions
no core complex
core complex formation
Tirel et al., 2008
Huet et al., 2011
Rey et al., 2009

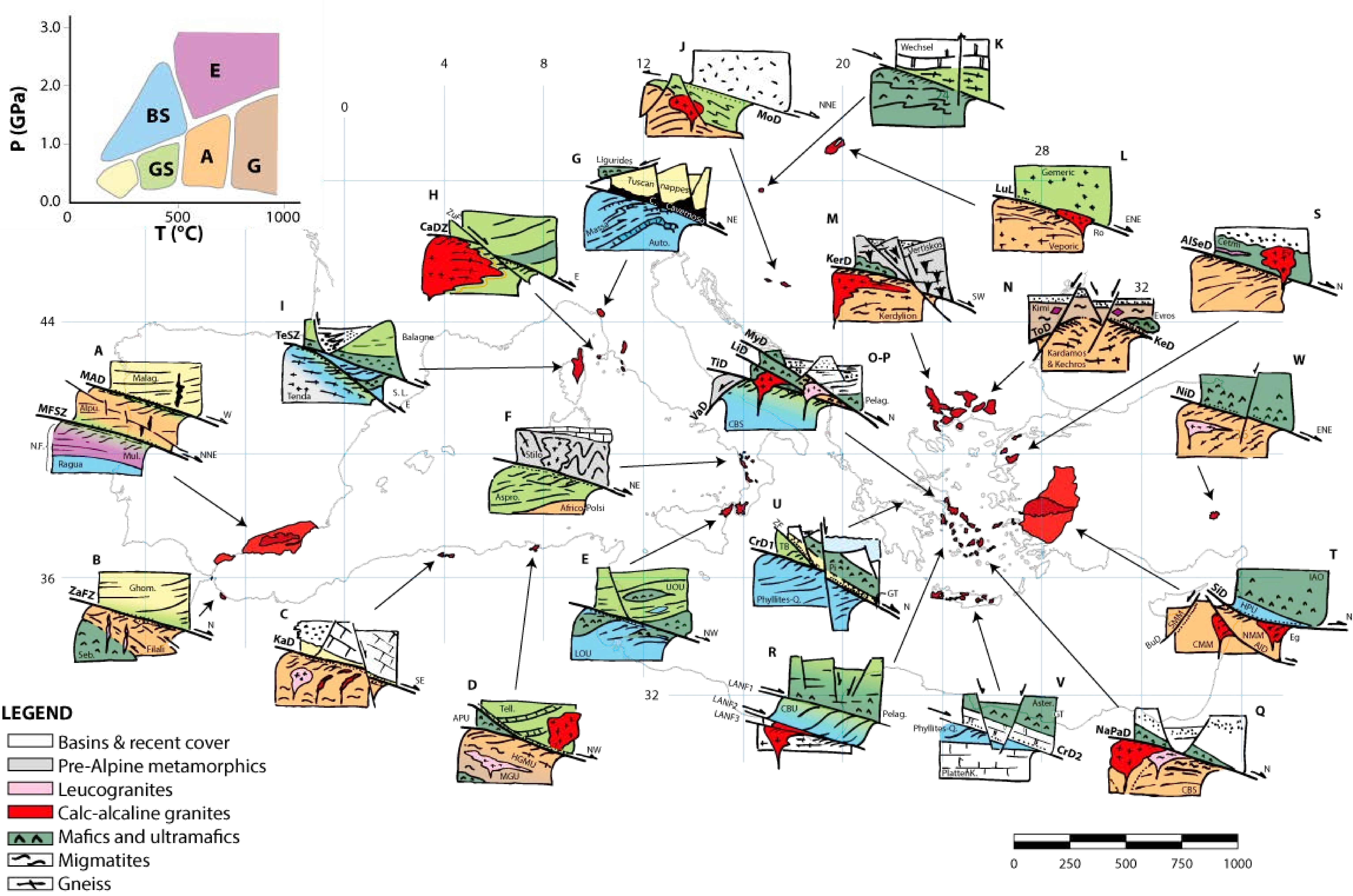

3.0
2.0
1.0
0.0
P (GPa)
0
500
1000
T (°C)
E
BS
GS
A
G
0
4
8
12
20
28
32
44
36
32
A
MAD
Malag.
Alpu.
MFSZ
N.F.
Mul.
Ragua
W
NNE
B
ZaFZ
Ghom.
Seb.
Filali
N
C
KaD
SE
D
Tell.
APU
HGMU
MGU
NW
E
UOU
LOU
NW
F
Stilo
Aspro.
Africo-Polsi
NE
G
Ligurides
Tuscan
nappes
Cavernoso
Massa
Auto.
NE
H
CaDZ
E
I
TeSZ
Balagne
Tenda
S. L.
E
J
MoD
NNE
K
Wechsel
L
LuL
Gemeric
Veporic
Ro
ENE
M
KerD
Vertiskos
Kerdylion
SW
N
Kimi
ToD
Evros
KeD
Kardamos
& Kechros
O-P
MyD
LiD
TiD
VaD
CBS
Pelag.
N
S
AlSeD
Cetm
N
W
NiD
ENE
T
SiD
IAO
HPU
SMM
BuD
CMM
NMM
AlD
Eg
N
U
CrD1
TB
Phyllites-Q.
GT
N
R
LANF1
LANF2
LANF3
CBU
Pelag.
V
Aster.
GT
Phyllites-Q.
CrD2
PlattenK.
Q
NaPaD
CBS
N
LEGEND
Basins & recent cover
Pre-Alpine metamorphics
Leucogranites
Calc-alcaline granites
Mafics and ultramafics
Migmatites
Gneiss
0
250
500
750
1000

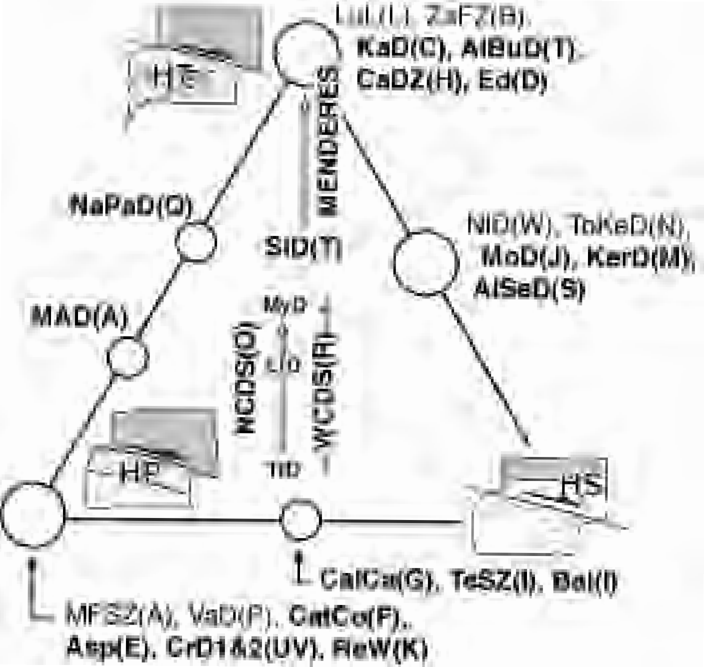

KaD(C), AlBuD(T),
CaDZ(H), Ed(D)
HT
MENDERES
NaPaD(O)
SlD(T)
NlD(W), ToKeD(N),
MoD(J), KerD(M),
AlSeD(S)
MAD(A)
MyD
NCDS(Q)
WCDS(R)
TID
HP
HS
CalCa(G), TeSZ(I), Bel(I)
MFSZ(A), VaD(P), CatCa(F),
Asp(E), CrD1&2(UV), ReW(K)

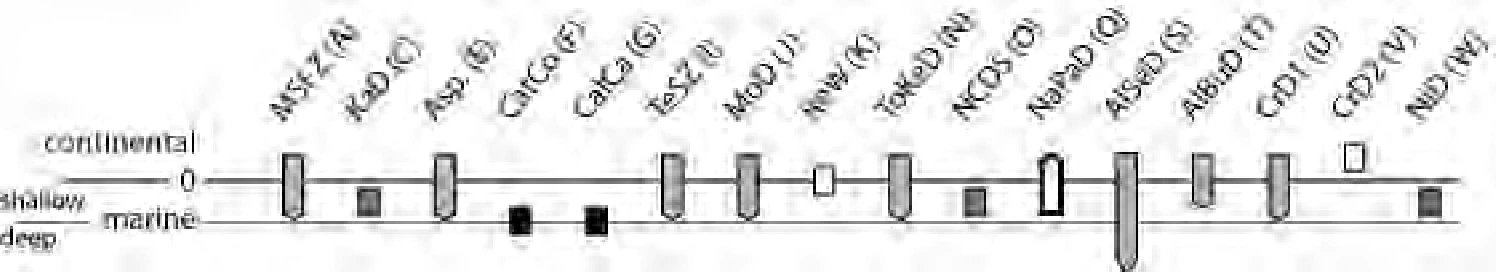

MSFZ (A)
KaD (C)
Asp. (E)
CarCo (F)
CalCa (G)
TeSZ (I)
MoD (J)
ToKeD (N)
NCOS (O)
NaPaD (Q)
AlSeD (S)
CrD1 (U)
CrD2 (V)
NiD (W)
continental
0
shallow
marine
deep

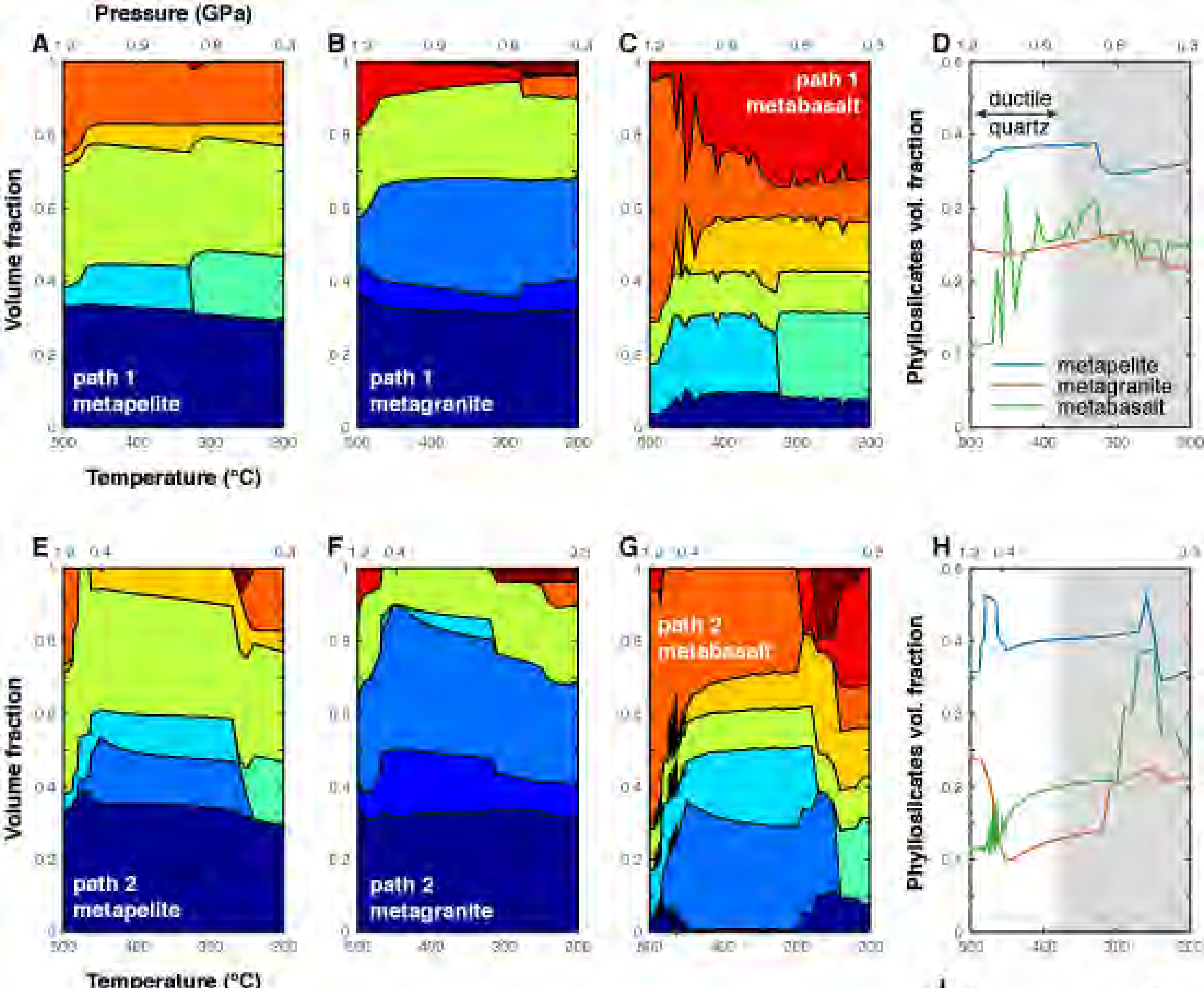

I

	SiO_2	Al_2O_3	Fe_2O_3	FeO	MgO	CaO	Na_2O	K_2O
Pelite (B85)	63.31	17.22	0.82	5.45	3.00	3.52	1.48	3.64
Granite (LM76)	71.84	14.43	1.22	1.65	0.72	1.85	3.71	4.00
Basalt (LM76)	49.97	15.99	3.85	7.00	6.84	9.82	2.96	1.12

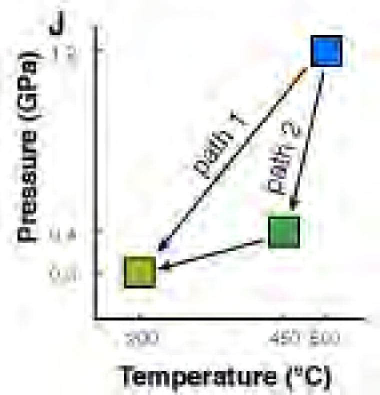

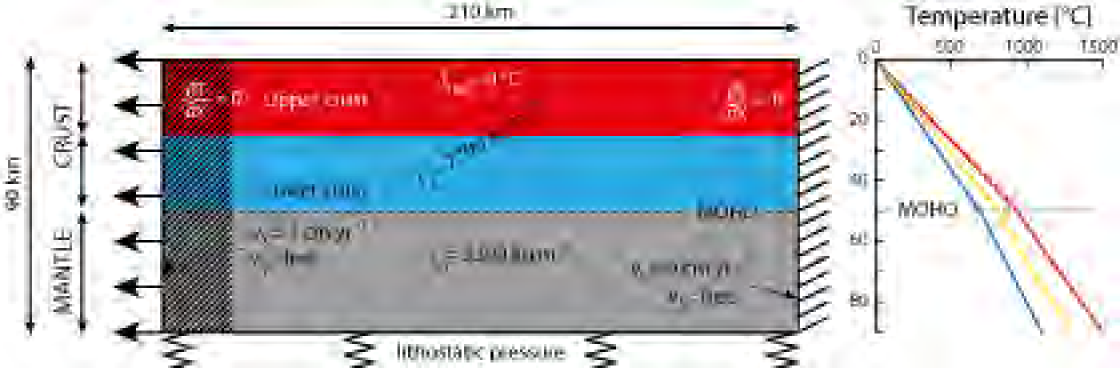

210 km
Temperature [°C]
0
500
1000
1500
20
40
60
80
CRUST
MANTLE
90 km
MOHO
lithostatic pressure

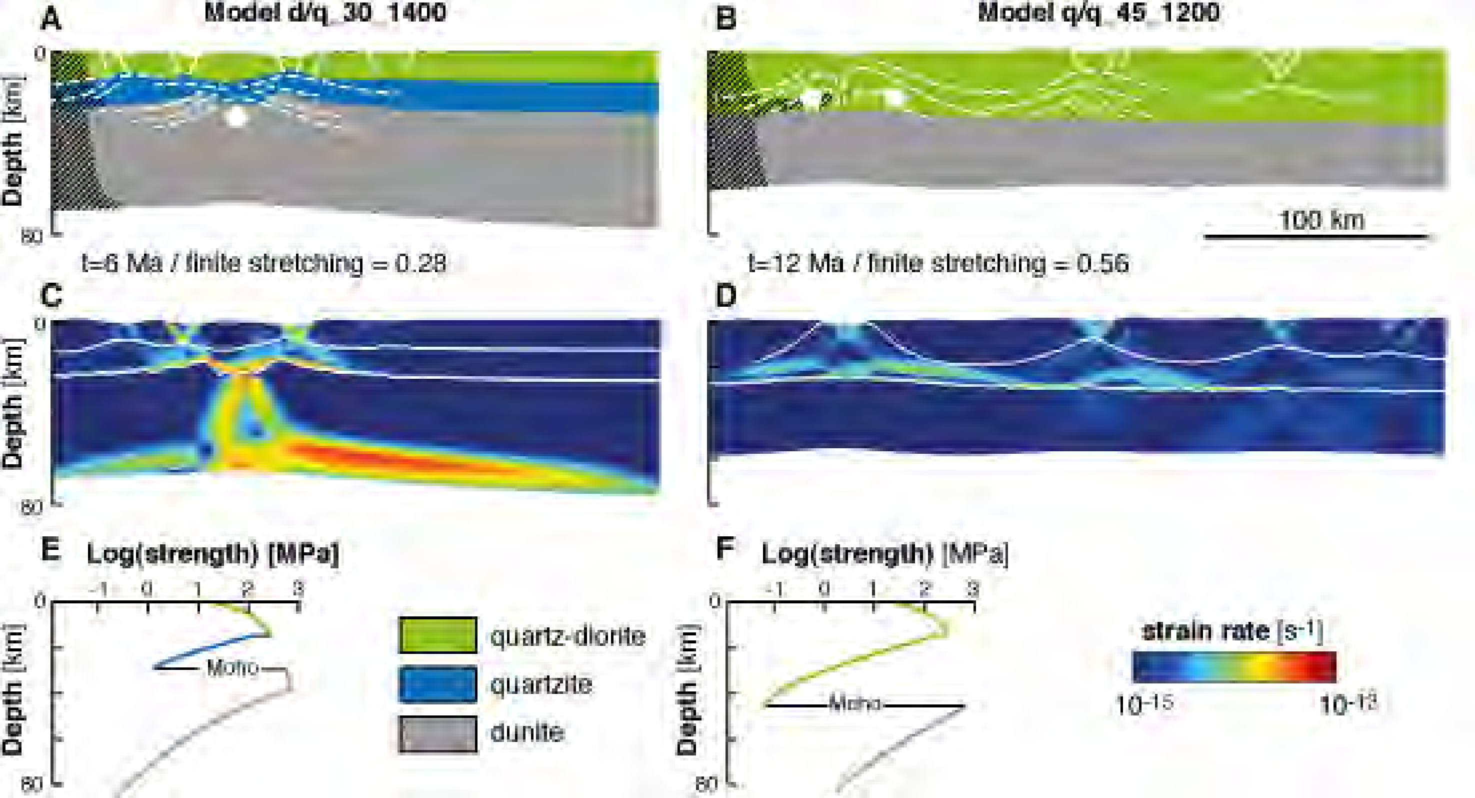

A
Model d/q_30_1400
B
Model q/q_45_1200
Depth [km]
0
80
100 km
t=6 Ma / finite stretching = 0.28
t=12 Ma / finite stretching = 0.56
C
D
E
Log(strength) [MPa]
-1 0 1 2 3
Moho
F
quartz-diorite
quartzite
dunite
strain rate [s-1]
10-15
10-13

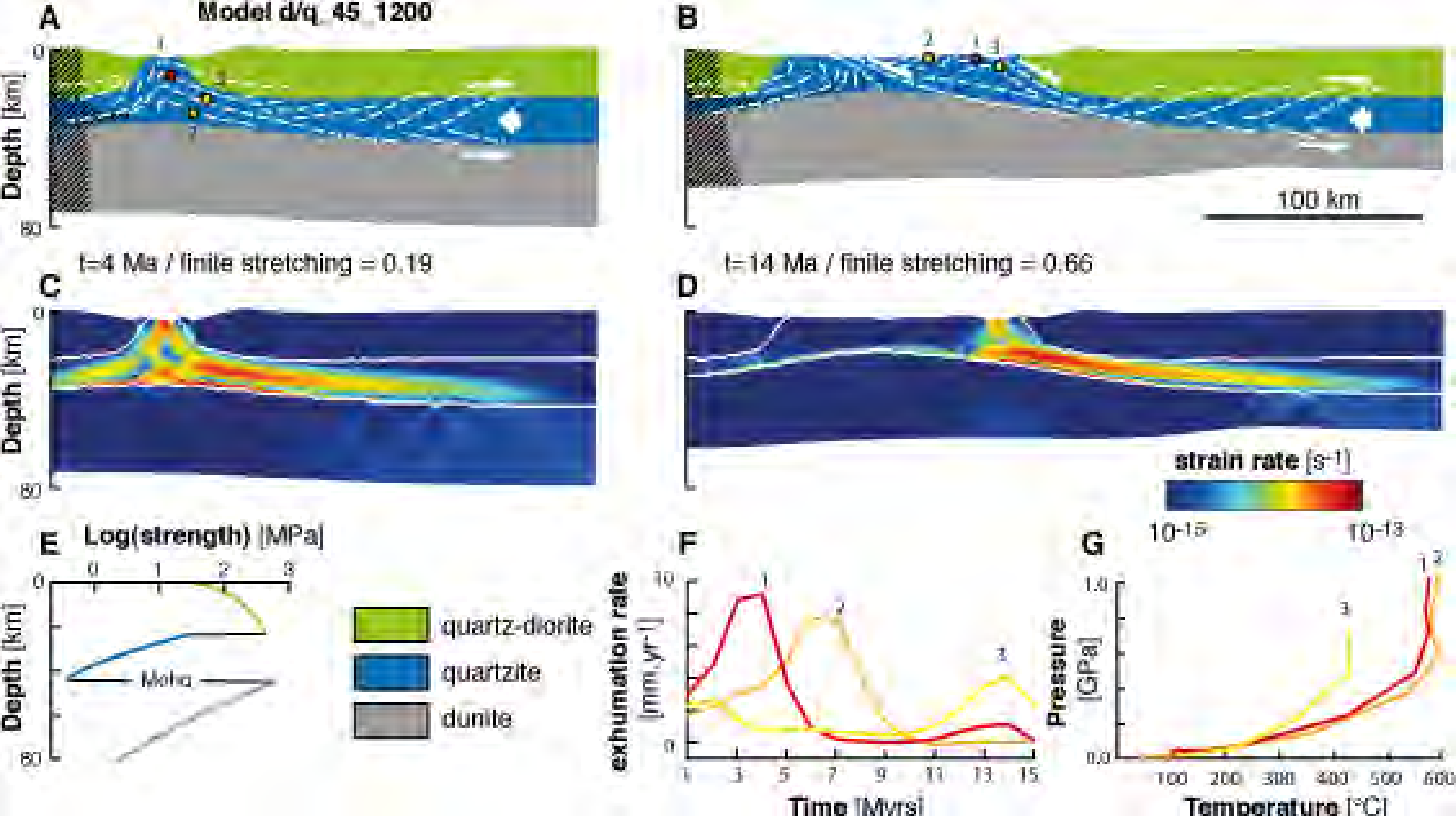

A
Model d/q_45_1200
B
Depth [km]
0
80
100 km
t=4 Ma / finite stretching = 0.19
t=14 Ma / finite stretching = 0.66
C
D
strain rate [s-1]
10-15
10-13
E
Log(strength) [MPa]
0
1
2
3
Moho
quartz-diorite
quartzite
dunite
F
exhumation rate [mm.yr-1]
Time [Myrs]
G
Pressure [GPa]
1.0
0.0
Temperature [°C]
100
200
300
400
500
600

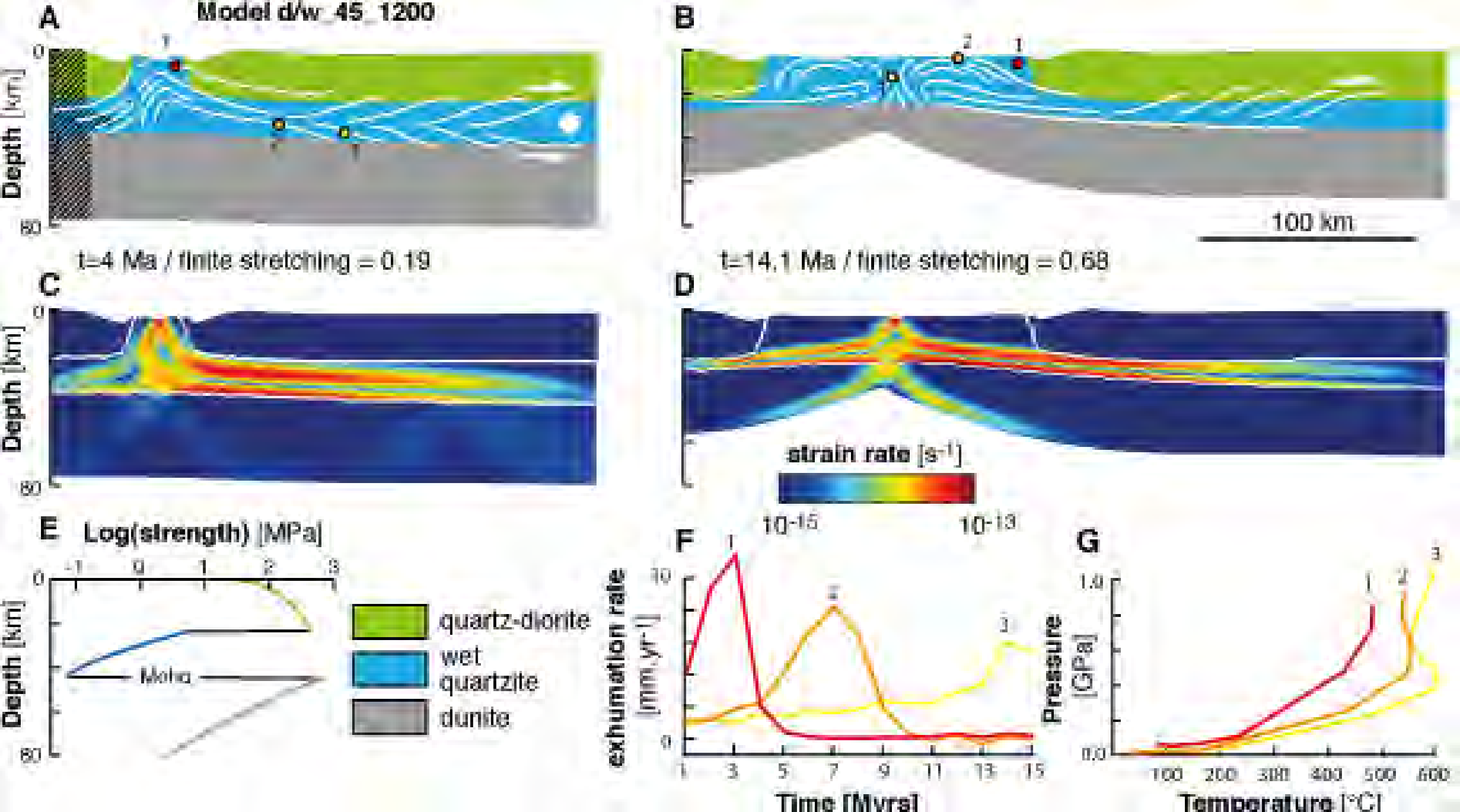

Model d/w_45_1200
A
B
Depth [km]
0
80
1
2
100 km
t=4 Ma / finite stretching = 0.19
t=14.1 Ma / finite stretching = 0.68
C
D
strain rate [s-1]
10-15
10-13
E
Log(strength) [MPa]
-1
0
1
2
3
Moho
quartz-diorite
wet quartzite
dunite
F
exhumation rate [mm yr-1]
10
0
Time [Myrs]
1
3
5
7
9
11
13
15
G
Pressure [GPa]
1.0
0.0
Temperature [°C]
100
200
300
400
500
600

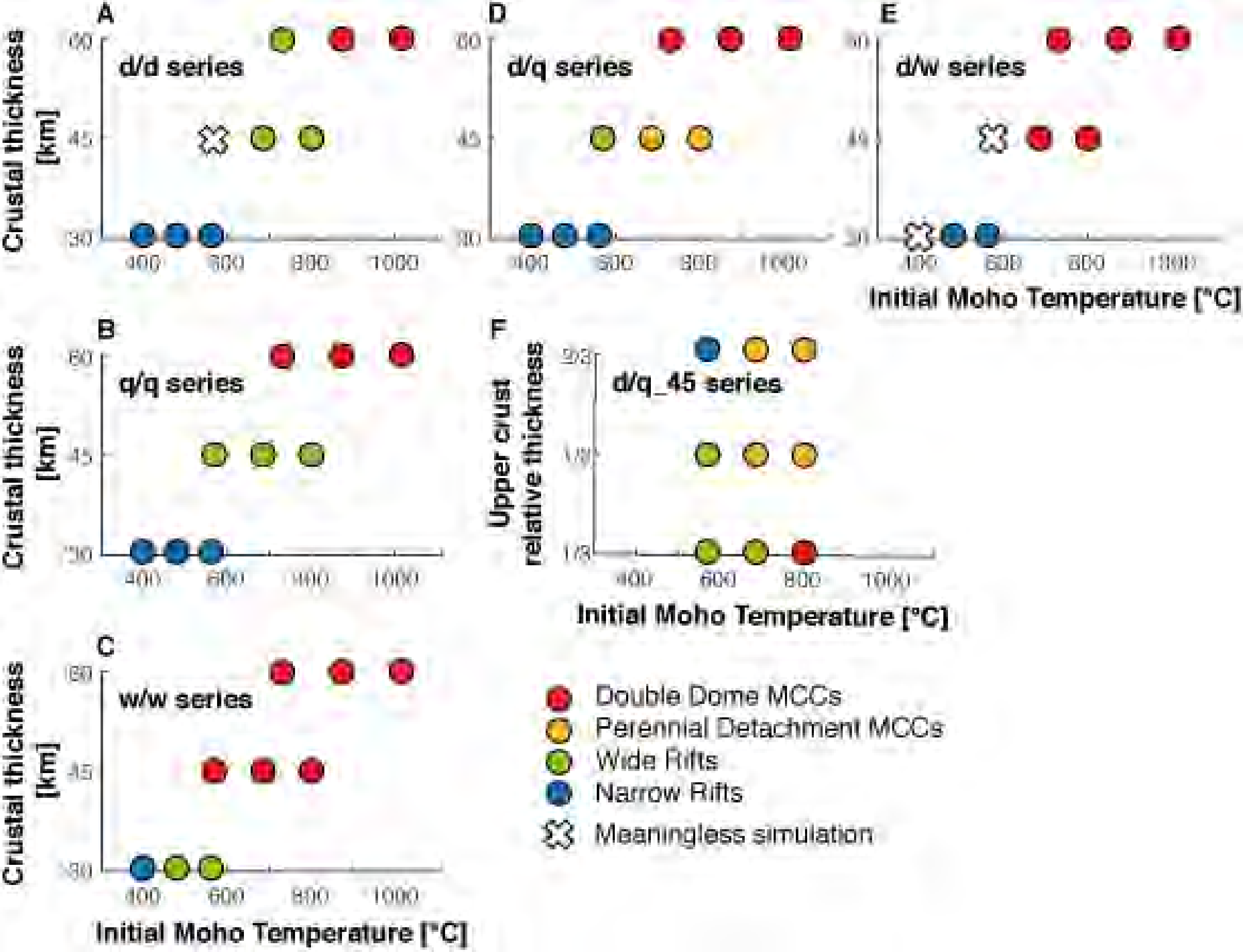

A
d/d series
B
q/q series
C
w/w series
D
d/q series
E
d/w series
F
d/q_45 series
Crustal thickness [km]
60
45
30
Upper crust relative thickness
2/3
1/2
1/3
400
600
800
1000
Initial Moho Temperature [°C]
Double Dome MCCs
Perennial Detachment MCCs
Wide Rifts
Narrow Rifts
Meaningless simulation

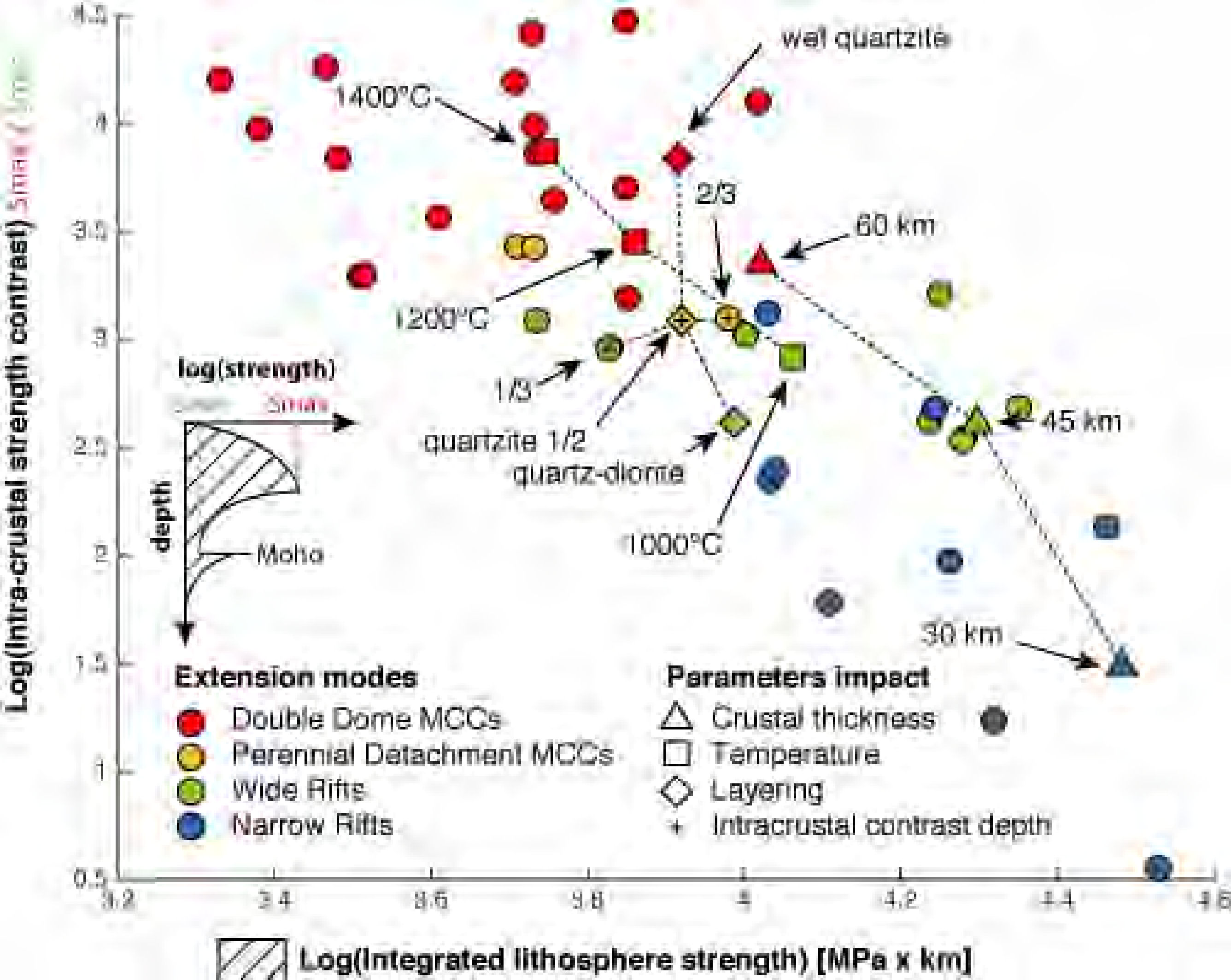

Log(Intra-crustal strength contrast)
Log(Integrated lithosphere strength) [MPa x km]
wet quartzite
1400°C
1200°C
1000°C
2/3
1/3
60 km
45 km
30 km
quartzite 1/2
quartz-diorite
log(strength)
depth
Moho
Extension modes
Double Dome MCCs
Perennial Detachment MCCs
Wide Rifts
Narrow Rifts
Parameters impact
Crustal thickness
Temperature
Layering
Intracrustal contrast depth

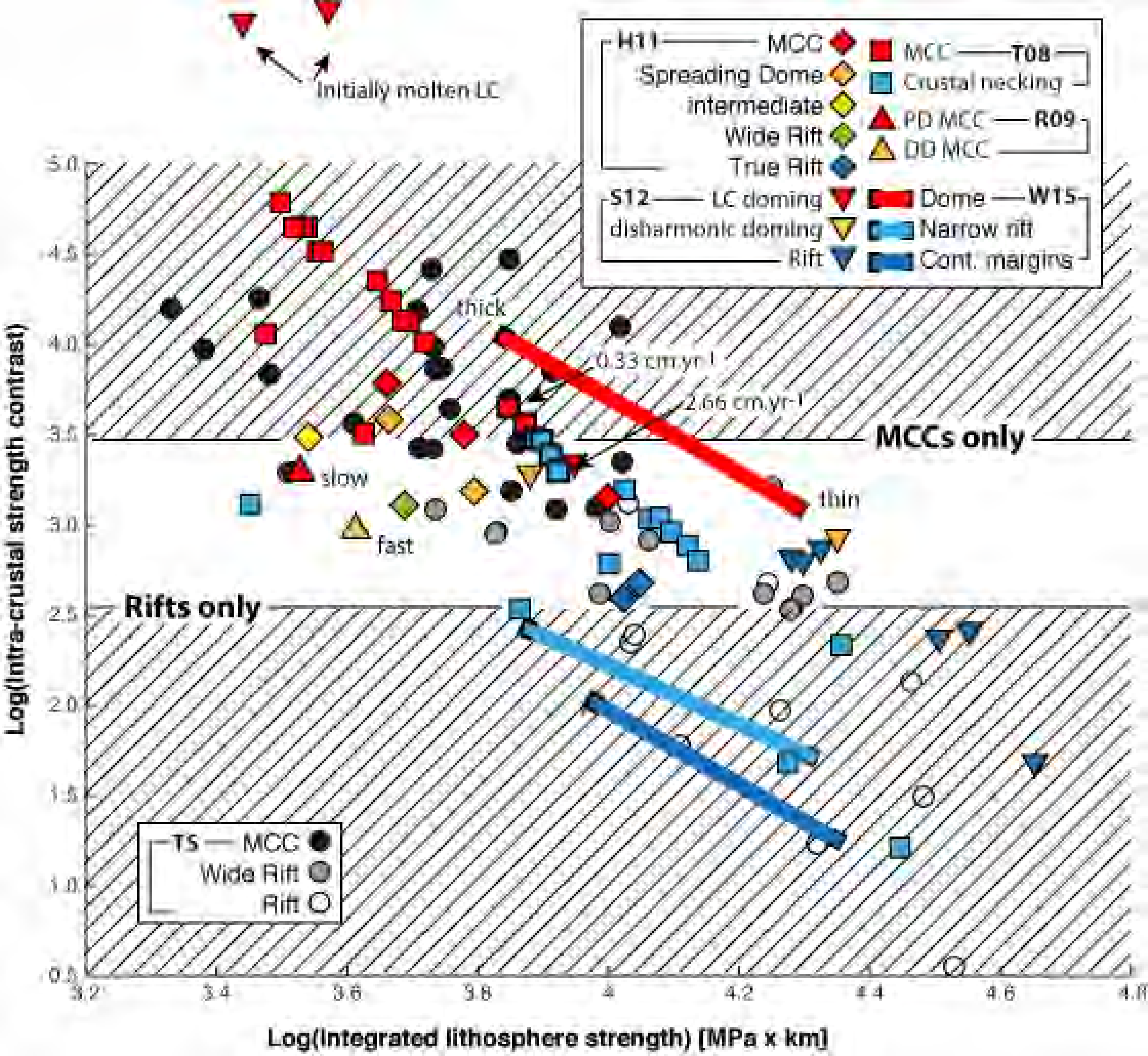

Initially molten LC
H11
MCC
Spreading Dome
intermediate
Wide Rift
True Rift
MCC
T08
Crustal necking
PD MCC
R09
DD MCC
S12
LC doming
disharmonic doming
Rift
Dome
W15
Narrow rift
Cont. margins
thick
0.33 cm.yr-1
2.66 cm.yr-1
MCCs only
slow
fast
thin
Rifts only
TS
MCC
Wide Rift
Rift
Log(intra-crustal strength contrast)
Log(integrated lithosphere strength) [MPa x km]

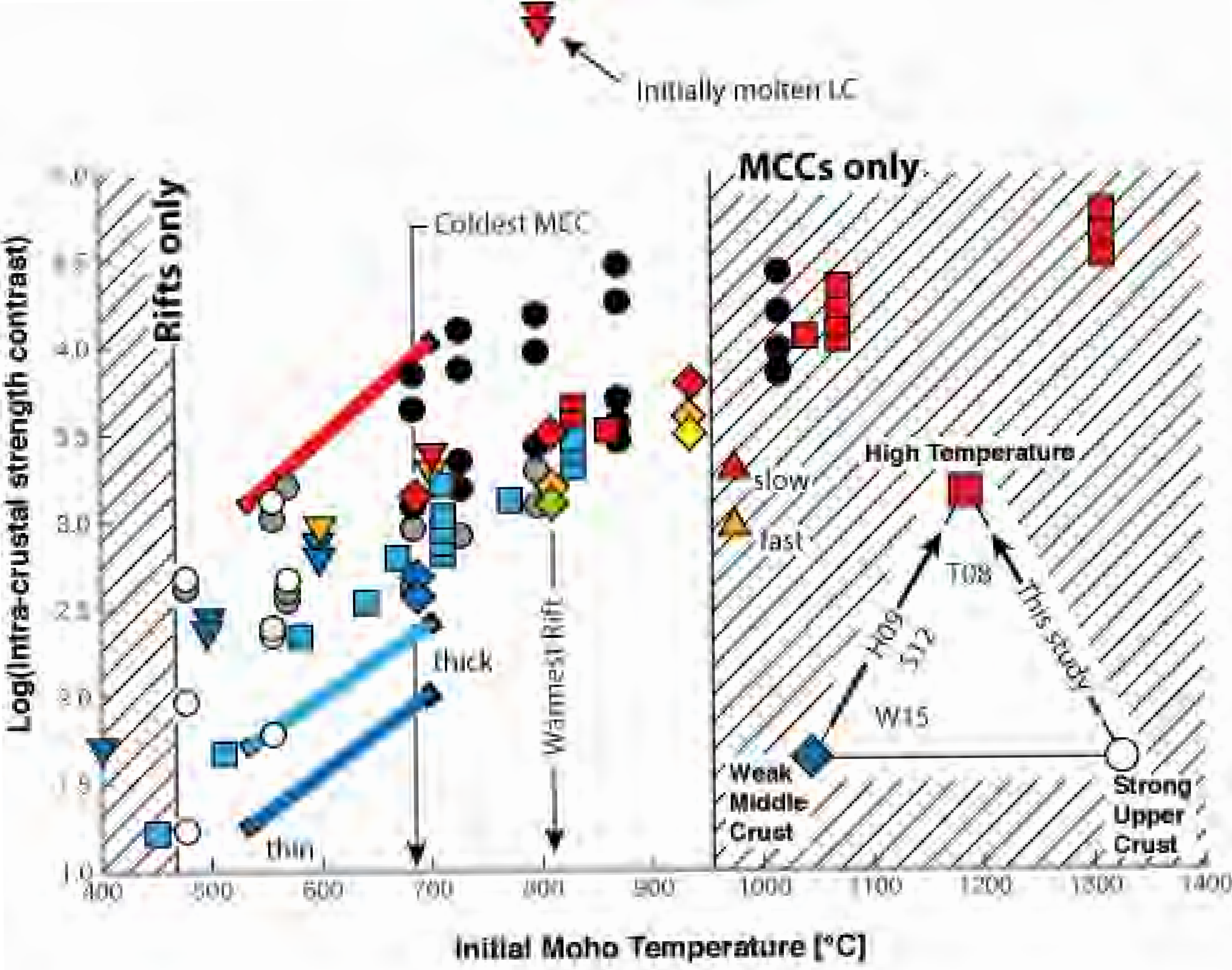

Initially molten LC
Rifts only
MCCs only
Coldest MCC
Warmest Rift
thick
thin
slow
fast
High Temperature
T08
H09
S12
This study
W15
Weak Middle Crust
Strong Upper Crust
Log(Intra-crustal strength contrast)
Initial Moho Temperature [°C]

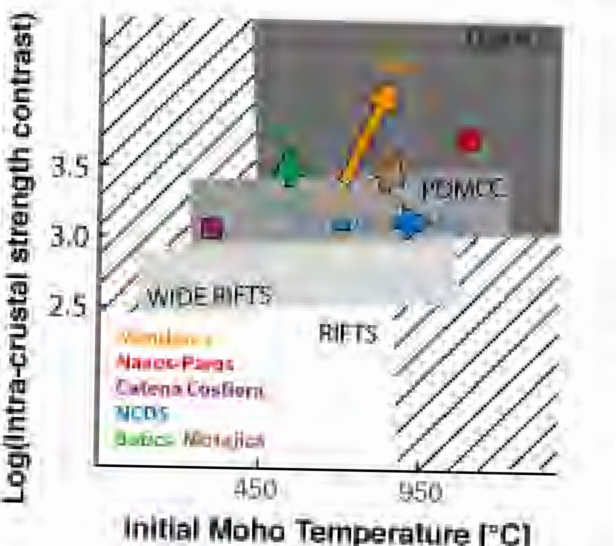

Log(Intra-crustal strength contrast)
3.5
3.0
2.5
PDMCC
WIDE RIFTS
RIFTS
Naxos-Paros
NCDS
450
950
Initial Moho Temperature [°C]

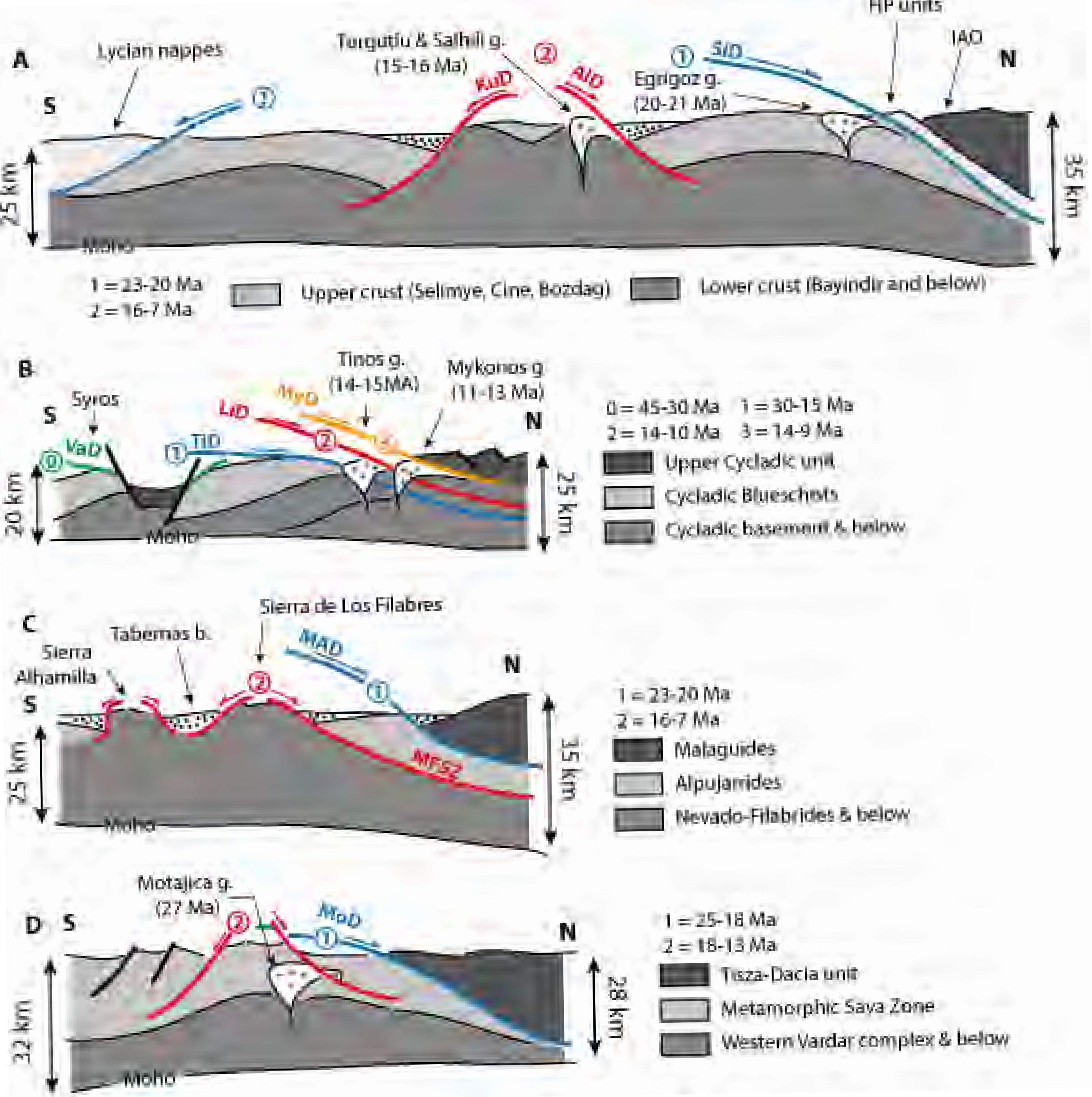
A
Lycian nappes
Turgutlu & Salhili g.
(15-16 Ma)
HP units
IAO
N
S
SiD
KuD
AlD
Egrigoz g.
(20-21 Ma)
25 km
35 km
Moho
1 = 23-20 Ma
2 = 16-7 Ma
Upper crust (Selimye, Cine, Bozdag)
Lower crust (Bayindir and below)
B
Syros
Tinos g.
(14-15MA)
Mykonos g.
(11-13 Ma)
S
N
VaD
TiD
LiD
MyD
20 km
25 km
Moho
0 = 45-30 Ma
1 = 30-15 Ma
2 = 14-10 Ma
3 = 14-9 Ma
Upper Cycladic unit
Cycladic Blueschists
Cycladic basement & below
C
Sierra Alhamilla
Tabernas b.
Sierra de Los Filabres
MAD
N
S
MFSZ
25 km
35 km
Moho
1 = 23-20 Ma
2 = 16-7 Ma
Malaguides
Alpujarrides
Nevado-Filabrides & below
D
S
Motajica g.
(27 Ma)
MoD
N
32 km
28 km
Moho
1 = 25-18 Ma
2 = 18-13 Ma
Tisza-Dacia unit
Metamorphic Sava Zone
Western Vardar complex & below

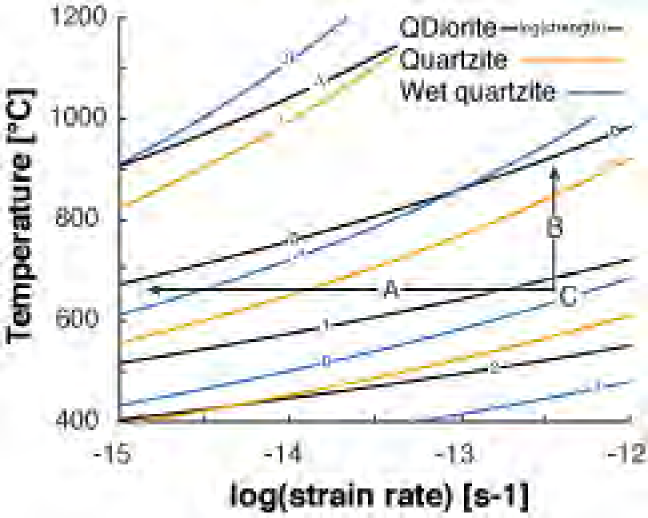

QDiorite
Quartzite
Wet quartzite
A
B
C
1200
1000
800
600
400
-15
-14
-13
-12
Temperature [°C]
log(strain rate) [s-1]

Site	minimum pressure (kb)	maximum pressure (kb)
SABN	8	10
GK	3	5
Edough	12	14
Tenda		
Beni Mesala	13	18
Filali		
BB kinzigites	9	13
BB mafic	16	20
Catena Costiera	11	13
Apuane Auto	7	9
Apuane Massa	8	11
argentario	11	13
aspromonte	11,2	12,4
alpu LG		7
alpu Es	6,5	8,5
alpu He	10	12
alpu S & A	7	11
NF BM	18	20
NF CA	11	15
NF beginning D3	3	4
Menderes Selimye	4	8
Menderes Bozdag		
Menderes Cine HP		
Menderes Cine HT		
Erhodope HP	13	15
Erhodope HT	3	9
Thasos	6,5	9,5
kazdag	4	6
Nigde Gumusler	5	6
andros post-orogen	6	8
Ikaria	6	8
tinos (transition)	8	10
tinos (late)	0	2
tinos HP	15	18
tinos BS	8	13
syros HP	16	20
syros retrogression	3	6
ios overprint		
ios peak basement	15	18
naxos	4,5	9,5
rechnitz HP	6	8
rechnitz late	3	4
veporic	9	10
Motajica	5	7

minimum T (°C)	maximum temperature (°C)	average pressure (kb)
660	700	
650	700	
600	800	
		9
450	550	
		8
800	850	
760	820	
	350	
410	430	
450	500	
350	400	
540	570	
	400	
	420	
540	620	
390	450	
550	650	
520	620	
		8
		15
		7
450	600	
550	620	
550	650	
590	690	
700		
600	650	
500	550	
400	500	
450	500	
375	525	
450	550	
300	450	
		8
480	520	
620	720	
330	370	
350	450	
550	630	

average temperature (°C)	Code	Timing	ref
	GK1	syn-detachment	saadallah96
	GK2	syn-detachment	"
	Ed	syn-detachment	caby01
400	Tn	syn-detachment	gueydan03
	BM	syn-detachment	negro 07
780	BB3	syn-detachment	"
	BB2	syn-detachment	"
	BB1	inherited	"
	CC	syn-detachment	rossetti04
	AA2	syn-detachment	jolivet98
	AA1	inherited	"
	Arg	syn-detachment	brunet00
	Asp	syn-detachment	ortolano05
	Alpu4	syn-detachment	azanon00
	Alpu3	inherited	"
	Alpu1	inherited	"
	Alpu2	inherited	"
	NF1	inherited	augier05
	NF2	inherited	"
500	NF3	syn-detachment	"
550	Me4	syn-detachment	whitney02 / Regnier 03
530	Me3	syn-detachment	okay01
640	Me1	inherited	oberhansli&al in press
620	Me2	syn-detachment	"
	Rho1	inherited	bonev & beccaletto07
	Rho2	syn-detachment	"
	Rho3	syn-detachment	brun & sokoutis07
	Kaz	syn-detachment	cavazza09
	Nig	syn-detachment	Whitney & Dilek, 98
450	And	syn-detachment	huet phd
		syn-detachment	Laurent 2016
	Tin3	syn-detachment	parra 02
	Tin4	syn-detachment	"
	Tin1	inherited	"
	Tin2	inherited	"
	Syr1	inherited	trotet 01
	Syr2	syn-detachment	huet phd
400	Ios1	syn-detachment	huet phd
	Ios2	inherited	huet phd
	Nax	syn-detachment	buick & holland 89
	Rech1	inherited	koller 85
	Rech2	syn-detachment	"
620	Vep	syn-detachment	janak 01
	Mot	syn-detachment	Ustaszewski10